DEFECTED SIGNAL LINE STRUCTURES FOR SINGLE-BAND AND MULTI-BAND BANDSTOP FILTERING IN PLANAR MICROWAVE DEVICES

by

Navneet Kumar Yadav

A thesis submitted to the faculty of
The University of North Carolina at Charlotte
in partial fulfillment of the requirements
for the degree of Master of Science in
Electrical Engineering

Charlotte

2018

Approved by:

_____
Dr. Ryan Adams

_____
Dr. Thomas Weldon

_____
Dr. Tao Han

ABSTRACT

NAVNEET KUMAR YADAV. Defected signal line structures for single-band and multi-band bandstop filtering in planar microwave devices. (Under the direction of DR. RYAN ADAMS)

As the development of wireless communication increases, the current transceiver architectures also needs to be evolving along with it. This results in specifications like high linearity, low noise figure, and rejection of spurious signals. As devices becoming more and more compact there is a need for high integration density by miniaturization of components, with multiple band operation. All these requirements translate the need to miniaturize bandstop filters which also have a multiband response and suppress higher order harmonics.

This document shows a novel concept of using the Defected structures on signal lines to provide a solution for above-mentioned challenges. These structures are similar to Defected ground structures (DGS), but they are etched on the signal line. Since 1980‘s, Defected ground structures were being used to get compact size, suppression of harmonics and arbitrary stopband. These structures were well analyzed and have established the equivalent model. In order to develop this theory, the frequency characteristics of defected signal line structure were compared to DGS, as well as the method for parameter extraction. Analysis has shown that evaluation and parameter extraction of defected signal line structure is similar to DGS. A novel G-shaped structure was also introduced and evaluated to get higher inductance and capacitance in a smaller area. At the end, these defected signal line structures (DSS) were integrated with single section Wilkinson power divider to achieve bandstop filtering and multiband response. The impact on resonance frequency by changing the dimensions were also examined for tuning the desired frequency response. These structures were simulated in HFSS and fabricated on FR4 board.

DEDICATION

This work is solely dedicated to my advisor, Dr. Ryan Adams, who inspired me to achieve my goals and introduced me to the world of Electromagnetism.

ACKNOWLEDGEMENTS

I would like to express my deepest gratitude to my parents,for having faith in me and supported me in my ups and down in life. I am grateful to all of my friends and faculty at UNCC for supporting me and making this journey memorable. I bow down to God and thank him for blessing me with all these peoples and great opportunities.

TABLE OF CONTENTS

LIST OF TABLES

LIST OF FIGURES

CHAPTER 1: INTRODUCTION

The demand for number of mobile devices, data rates and connectivity is increasing on a day to day basis. Due to evolution of Internet of Things, which needs 5G network, the mobile handset is required to do many applications with different standards using different technologies. Figure 1.1 shows the current applications along with it's enabling technologies.

(a)

Figure 1.1: Various mobile applications along with its enabling technology[1].

It shows that the mobile device is capable of handling the frequency spectrum from low frequency GSM 800 MHz for GPS up to frequency as high as 6 GHz for IEEE802.11a for Wi-Fi applications. Considering these changes, it is expected of a mobile device to operate in wide frequency range. The device should also be compatible with multi standards like Bluetooth, GSM ,Wi-Fi, LTE etc. with minimum interference among the adjacent bands. It is also moving towards less power consumption, and a compact size to keep up with the current trend. All these demands

should also account for cost effectiveness within the market. Figure 1.2 shows the architecture of mobile device which contains several active and passive components.

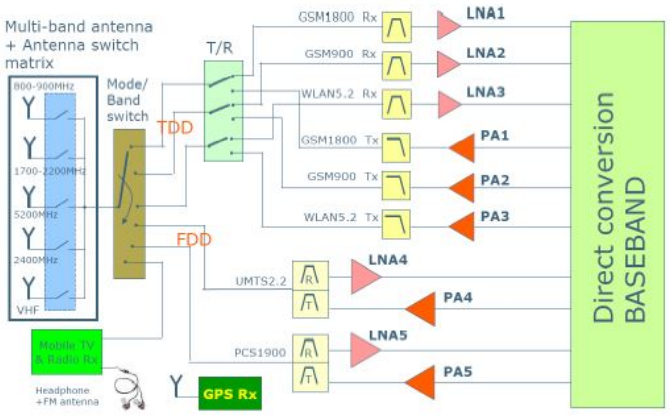

(a)

Figure 1.2: Architecture of mobile device [1]

They are responsible for acquiring 80 % of space in printed circuit board and 70% of the cost. A common technique to achieve bandstop response in industry is using LC circuit, which creates a notch at desired frequency, but the inductor acquires a huge dye area which directly impact the cost. So, the aim of the thesis is to integrate defected signal line structures with microwave circuits to attain single-band and multi-band bandstop response, which also achieves miniaturization of circuit.

1.0.1 Literature Review

Several design techniques like electromagnetic bandgap structures (EBG),defected ground structures (DGS) and power dividers with resonating stubs, were used to attain bandstop filtering and multi-band response. In the following section, some of them are briefly discussed.

In 1993, a planar antenna was designed with it's substrate made up of photonic crystal [2]. It was shown that due to periodic defects in the substrate, the electromagnetic wave cannot propagate in bandgap. In 1997, a comprehensive study on synthesizing

a dielectric material was performed to give bandstop response [3]. Four different kind of structures with square lattice,triangular lattice,Honeycomb square hole lattice and Honeycomb circular hole lattice were introduced for microstrip circuits. In 1998, same group of people proposed two dimensional photonic bandgap structures [4], in which the desired stopband response can be achieved by etching the metal from the ground plane. This process was simpler in fabrication as no drilling of holes was required. These attractive properties of and ease of fabrication, EBG structures were used in designing several active and passive divides like a power amplifier with EBG circuits [5],[6], the PBG structure for slow-wave circuits [7], and realization of a magnetic wall in waveguide [8], [9]; their experimental results are sufficient to show the validity of EBG circuit applications. However, the biggest issue with EBG was the complexity of equivalent model. It was difficult to extract parameters, as EBG has too many design parameters like number of lattice, lattice shape, lattice spacing and relative volume fraction. These problems with EBG helped in evolution defected ground structure [10],[11].

DGS has a simple equivalent circuit model [10]- [13] and only required one or two unit cell, compared to periodic structure, for desired frequency response. DSG can also have complex design for unit cell as the equivalent circuit model is simple. DGS research is going in two directions, first is in designing novel unit cell and second is in arranging these unit cell in a structure to get wide rejections or other interesting frequency responses. The losses in DGS are not included in its equivalent model o keep it simple. Parallel resistance was considered in [14]for suppression of harmonics in antenna design. In 1998, first DGS structure was introduced but was proposed as a photonic bandgap unit cell [54]. The paper presented equivalent circuit model of DGS as parallel LC circuit. The full wave EM simulation displayed a attenuation pole in scattering parameters, which proved the existence of parallel LC. To show the legitimacy of extracted parameters and equivalent circuit, a three pole low pass filter

was designed. This was a seminal paper but it did not include the radiation losses and coupling between the adjacent DGS unit cell. In 2000, DSG term was started to appear for the first time [16], [17]. A Dumbell shaped DGS was examined to increase the effective inductance and shift the resonating frequency. It was also shown that the DSG has bandstop filtering response, which depends on its dimensions. At the end of same year, the application of DGS as 10 db branch line coupler [17] was introduced. Application of DGS were not limited to passive device, in 2001 DGS was used to increase the efficiency of power amplifier [18]. The DGS suppress second order harmonic, which resulted in increase of 1 to 5 % of power efficiency. In 2002, a more complex equivalent circuit model was proposed for more accurate parameter extraction [19]. It introduced parallel capacitance to model fringing fields due to DGS. It was in the form of π. This model was more accurate but generally, RLC model is preferred by researchers due to there simplicity and reasonable accuracy in designing the circuits. In 2005, cascaded U-shaped DGS was used to achieve wide rejection in stopband [20]. This paper showed to view DGS as a block element and interesting filtering response can be achieved by cascading it or combining in certain fashion. Spiral DGS were introduced in 2002 [21]. The spiral DGS provide rapid increase in effective inductance and slow wave effects compared to other DGS. Another application was shown by Woo an Lee , in 2005 when second and third harmonics were suppressed by using asymmetric spiral DGS [22]. In order to achieve multiband rejection, stacked spiral DGS and composite spiral-rectangular DGS were used [23]. On the other hand the vertically periodic defected ground structure were used organize periodicity in vertical direction and to achieve higher slow-wave factor compared to other DGS [24]. The first two reconfigurable DGSs appeared in 2005. The first is by Kim from the Korea University, for the implementation of tunable bandstop filter [33] and the other by Mansour from Waterloo University, for the implementation of a tunable lowpass filter [34]-[35].

Till this moment novel DGS structures are emerging and with their equivalent circuit including parameters like losses due to radiation, conductor, dielectric and effects due to coupling in a quasi-static model [25] - [27]. On the other hand, not only new way of analyzing the equivalent circuit are emerging, different shapes of DGS were introduced like the U-shaped DGS [28], the cross-head DGS [31], the multilayer DGS [30], the arrow-head DGS [29] and the deformed DGS [32]. Every structure has its own advantages like reduced size, narrow stopband response, minimum loss and better coupling.I tried to cover the most important work that has been published in this area. The bandgap structures are advancing at a great pace towards accurate way of analyzing equivalent circuit and better characteristics.

CHAPTER 2: BACKGROUND ON EM THEORY AND MICROWAVE CIRCUITS

2.1 Introduction to Microwave Engineering

The range of spectrum covered by radio frequency (RF) and microwave engineering is from 100 MHz to 1000 GHz. The frequency range can be further categorized for microwave to be in between 3 to 300 GHz, with the corresponding wavelength between $\lambda = c/f = 10$ cm and $\lambda = 1$ mm, respectively, where c is the speed of light. The location of RF and microwave frequency bands in electromagnetic spectrum are shown in figure 2.1 . Standard circuit theory that is used to analyze lumped circuit model does not apply in the analysis of microwave circuits, as they operate at such high frequencies where the circuit size is comparable to the wavelength. As the circuit size is proportional to signal wavelength, microwave components are modeled as distributive elements because the phase of voltage and current changes significantly over the size of the device. Lumped circuit model works for low frequencies, where the wavelength is large compared to device size, thus its appropriate to apply Kirchhoff's current and voltage laws. Maxwell's equations and their solutions are used to analyze circuits operating at RF and Microwave frequencies. [36].

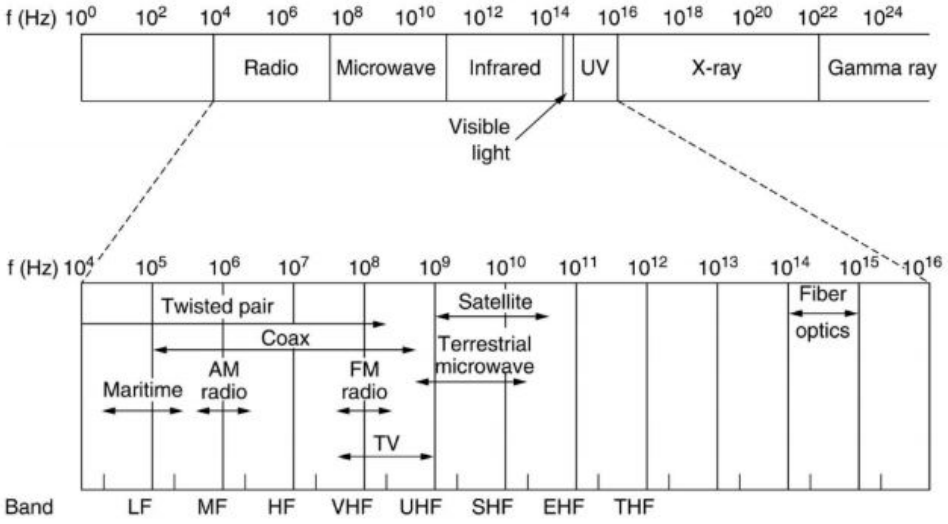

(a)

Figure 2.1: The electromagnetic spectrum [36]

2.2 Maxwell Equations

Maxwell's equations are set of partial differential equations that forms the foundation of classical electromagnetism and microwave circuits. These equations shows, how charges and current affect the electromagnetic fields as well as the interdependencies of electric and magnetic fields. The equations are named after the physicist and mathematician James Clerk Maxwell, who published the macroscopic analysis of this work in 1873. Boundary value electromagnetic problems are most commonly solved by using the differential form of Maxwell Equations, which shows the relationship of field vectors, current densities, and charge densities at any point in space at any time. In differential form, Maxwell's equations can be written as [36]

$$\nabla \times E = -\frac{\partial B}{\partial t} - M, \tag{2.1}$$

$$\nabla \times H = \frac{\partial D}{\partial t} + J, \tag{2.2}$$

$$\nabla . D = \rho, \tag{2.3}$$

$$\nabla . B = 0. \tag{2.4}$$

E is the electric field, in volts per meter (V/m) [38].

H is the magnetic field, in amperes per meter (A/m) .

D is the electric flux density, in coulombs per meter squared $(Coul/m^2)$.

B is the magnetic flux density, in webers per meter squared (Wb/m^2).

M is the (fictitious) magnetic current density, in volts per meter (V/m^2) .

J is the electric current density, in amperes per meter squared (A/m^2) .

ρ is the electric charge density, in coulombs per meter cubed $(Coul/m^3)$. The currents densities J,M and electric charge density ρ are responsible for fields, but the magnetic current used is just for simplifying the calculation, it's not an actual source. The scalar relation between the electric and magnetic field intensities are as follows

$$B = \mu_0 H \tag{2.5}$$

$$D = \epsilon_0 E \tag{2.6}$$

where, $\mu_0 = 4\pi \times 10^{-7}$ henry/m is the permeability of free-space, and $\epsilon_0 = 8.854 \times 10^{-12}$ farad/m is the permittivity of free-space.

2.3 Transmission Line Theory

The difference between standard circuit theory and transmission line theory is how the dimensions of component is comparable to the wavelength of the signal. As described before, the standard circuit theory analysis is performed on circuits where the size is relatively small compared to the wavelength, thus magnitude and phase are not affected along it's dimensions. While at higher frequencies the circuit dimensions are in the order of some fraction of wavelength, therefore; it is modeled as distributive component which changes in phase and magnitude along it's dimensions [36].

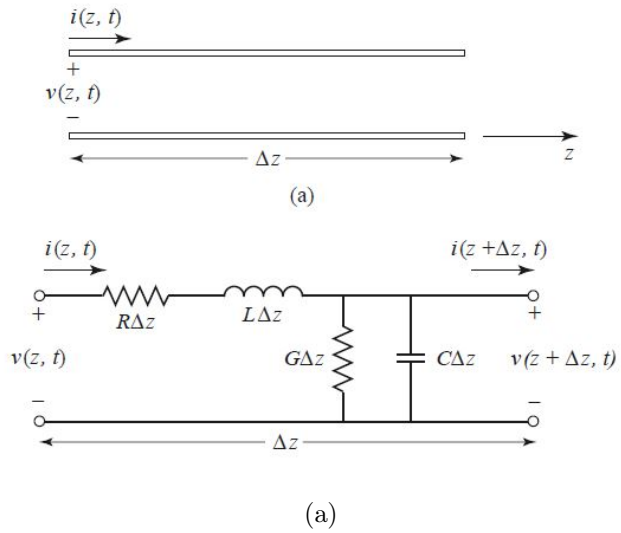

Figure 2.2: Voltage, Current and Lumped-element equivalent circuit [36]

As shown in figure 2.2, a two line model is used to represent transmission line, since transverse electromagnetic waves requires a representation of at least two conductors. This model can be analyzed using standard circuit theory by considering it as a lumped component, under a condition when ΔZ is infinitesimal length. Due to the distributive nature of the model the resistance R, inductance L, capacitance C are quantified per unit length.

R = series resistance per unit length, for both conductors, in Ω/m

L = series inductance per unit length, for both conductors, in H/m.

G = shunt conductance per unit length, in S/m.

C = shunt capacitance per unit length, in F/m.

The inductance shown in series is due to the self inductance of two conductors while the capacitance is based upon closeness between the conductors. The series resistance and shunt conductance are due to the losses associated with conductor and dielectric, respectively. By applying Kirchhoff's voltage law on the circuit shown in Figure 2.2, gives [36]

$$\upsilon(z,t) - R\Delta z i(z,t) - L\Delta z \frac{\partial i(z,t)}{\partial t} - \upsilon(z+\Delta z,t) = 0, \tag{2.7}$$

and Kirchhoff's current law leads to

$$i(z,t) - G\Delta z v(z+\Delta z,t) - C\Delta z \frac{\partial v(z+\Delta z,t)}{\partial t} - i(z+\Delta z,t) = 0, \tag{2.8}$$

By dividing (2.7) and (2.8) by Δz and taking the limit as $\Delta z \longrightarrow 0$ gives the following differential equations:

$$\frac{\partial v(z,t)}{\partial z} = -Ri(z,t) - L\frac{\partial i(z,t)}{\partial t} \tag{2.9}$$

$$\frac{\partial i(z,t)}{\partial z} = -Gv(z,t) - C\frac{\partial v(z,t)}{\partial t} \tag{2.10}$$

These are also known as telegrapher equations [36]. These can be simplified to phasor form for steady-state condition.

$$\frac{dV(z)}{dz} = -(R + j\omega L)I(z) \tag{2.11}$$

$$\frac{dI(z)}{dz} = -(G + j\omega C)V(z) \tag{2.12}$$

2.4 Wave Propagation on a Transmission Line

Solution of two telegrapher equations leads to following wave equation for $V(z)$ and $I(z)$ [36]:

$$\frac{d^2V(z)}{dz^2} - \gamma^2 V(z) = 0 \tag{2.13}$$

$$\frac{d^2I(z)}{dz^2} - \gamma^2 I(z) = 0 \tag{2.14}$$

where,

$$\gamma = \alpha + j\beta = \sqrt{(R + j\omega L)(G + j\omega C)} \tag{2.15}$$

is a propagation constant with an imaginary part, which depends on frequency. The solution of traveling waves (2.13) and (2.14) is given by

$$V(z) = V_0^+ e^{-\gamma z} + V_0^- e^{\gamma z} \tag{2.16}$$

$$I(z) = I_0^+ e^{-\gamma z} + I_0^- e^{\gamma z} \tag{2.17}$$

where the wave propagation in the +Z direction is given by $e^{-\gamma z}$ term and the wave propagation in $-$Z direction is given by $e^{\gamma z}$ term. Applying (2.11) to the voltage of

(2.16) shows that the current in the line:

$$I(z) = \frac{\gamma}{R + j\omega L}(V_0^+ e^{-\gamma z} - V_0^- e^{\gamma z}) \tag{2.18}$$

by comparing (2.18) with (2.17), it was shown that the expression for the *characteristic impedance*, Z_0 [36] was :

$$Z_0 = \frac{R + j\omega L}{\gamma} = \sqrt{\frac{R + j\omega L}{G + j\omega C}} \tag{2.19}$$

where, Z_0 is the ratio of forward voltage wave to forward current wave and also, the ratio of negative backward voltage wave to backward current wave as shown below :

$$\frac{V_0^+}{I_0^+} = Z_0 = \frac{-V_0^-}{I_0^-} \tag{2.20}$$

Then (2.17) can be written as

$$I(z) = \frac{V_0^+}{Z_0} e^{-\gamma z} - \frac{V_0^-}{Z_0} e^{\gamma z} \tag{2.21}$$

The above expression [36] are general expressions for lossy and lossless transmission line. It has complex propagation constant and characteristic impedance which signifies lossy characteristics. Generally, the losses are small and can be ignored, which simplifies the above expressions (2.15) and (2.19). As a result, the series resistance and shunt conductance goes to zero and the propagation constant simplifies to :

$$\gamma = \alpha + j\beta = j\omega\sqrt{LC} \tag{2.22}$$

or

$$\beta = \omega\sqrt{LC} \tag{2.23}$$

$$\alpha = 0 \tag{2.24}$$

As shown in (2.24), the attenuation constant α is zero, reducing the characteristic impedance from (2.19) to :

$$Z_0 = \sqrt{\frac{L}{C}} \tag{2.25}$$

which shows that (2.25) is a real number and the solution for (2.16) and (2.17) for lossless transmission line is given as [36] :

$$V(z) = V_0^+ e^{-j\beta z} + V_0^- e^{j\beta z} \tag{2.26}$$

$$I(z) = \frac{V_0^+}{Z_0} e^{-j\beta z} - \frac{V_0^-}{Z_0} e^{j\beta z} \tag{2.27}$$

The wavelength is

$$\lambda = \frac{2\pi}{\beta} = \frac{2\pi}{\omega\sqrt{LC}} \tag{2.28}$$

and the phase velocity is

$$\upsilon_p = \frac{\omega}{\beta} = \frac{1}{\sqrt{LC}} \tag{2.29}$$

2.5 The Terminated Lossless Transmission Line

Figure (2.3) shows a lossless transmission line which is terminated by an unknown load Z_L and is not equal to characteristic impedance Z_0 of the transmission line. The characteristic impedance is not an actual resistance, which dissipate power. Its called impedance due to the ratio of forward voltage and forward current as mentioned in (2.20). It depends on the material property of the transmission line. The mismatch between the load Z_L and characteristic impedance Z_0 causes reflections in the transmission line. These reflections can be measured by reflection coefficient Γ, which is defined by the ratio of reflected wave to incident wave, where the magnitude was [36]

$$\Gamma = \frac{V_0^-}{V_0^+} \tag{2.30}$$

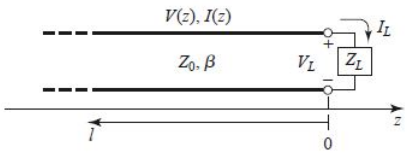

(a)

Figure 2.3: A transmission line terminated in a load impedance Z_L[36]

The value of characteristic impedance is different at different points in the line but it ia equal to Z_L at load, which is situated at origin. So, the magnitude of reflection coefficient Γ at load is given by [36]

$$\Gamma = \frac{V_0^-}{V_0^+} = \frac{Z_L - Z_0}{Z_L + Z_0} \tag{2.31}$$

Similarly, the general expression for reflection coefficient at any point along the T-line $Z = -l$ is:

$$\Gamma(l) = \frac{V_0^- e^{-j\beta l}}{V_0^+ e^{j\beta l}} = \Gamma(0) e^{-2j\beta l} \tag{2.32}$$

where $\Gamma(0)$ is the reflection coefficient at $z = 0$; and it is observed that by changing the length from 0 to $-l$ a phase term of $e^{-2j\beta l}$ is added to the expression.

The input impedance as a function of length of the transmission line looking towards the load at $Z = -l$ is [36] :

$$Z_{in} = \frac{V(-l)}{I(-l)} = \frac{V_0^+(e^{j\beta l} + \Gamma e^{-j\beta l})}{V_0^+(e^{j\beta l} - \Gamma e^{-j\beta l})} Z_0 \tag{2.33}$$

It can be further simplifies (2.33) to

$$Z_{in} = Z_0 \frac{Z_L + jZ_0 \tan \beta l}{Z_0 + jZ_L \tan \beta l} \tag{2.34}$$

This equation is known as transmission impedance equation [36] helps to calculate input impedance at any length with any arbitrary load. There are two special cases that are used for further analysis of transmission line input impedance. The first case applies short circuit at load i.e $Z_L = 0$, where the reflection coefficient is $\Gamma = -1$. By applying these two conditions in (2.34), the input impedance reduces to

$$Z_{in} = jZ_0 \tan \beta l \tag{2.35}$$

According to the (2.35) any value of impedance between $-j\infty$ to $+j\infty$ is achievable by adjusting the length of the line [36]. If $l = \lambda/4$ then the input impedance goes to infinity, therefore short circuited transmission line with quarter wave length behave as an open circuit. This quarter wave length plays a significant role in designing different microwave circuits.

In the second case, the load was an open circuit i.e $Z_L = \infty$, where the reflection coefficient was $\Gamma = 1$. Similarly, Using these conditions in (2.34), the input impedance reduces to [36]

$$Z_{in} = -jZ_0 \cot \beta l \tag{2.36}$$

So, at length $l = \lambda/4$ an open circuited transmission line behaves as a short circuit. Equation (2.35) also shows that the impedance was periodic function of l, where it repeated itself for the multiples of $\lambda/2$ as shown in figure 2.4. It was also evident from the Figure 2.4 that at a length of $l = \lambda/2$, the characteristic impedance remained the same i.e independent of the length

$$Z_{in} = Z_L \tag{2.37}$$

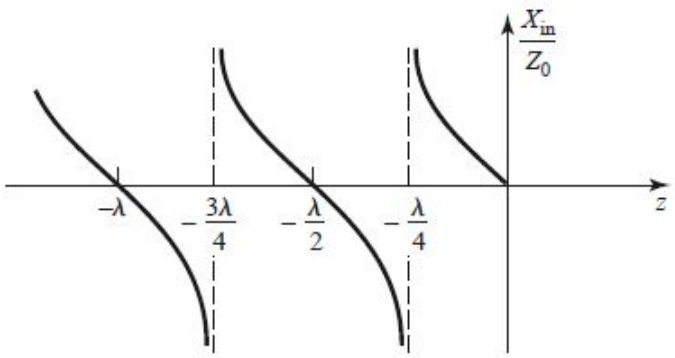

(a)

Figure 2.4: Impedance variation along a short circuited transmission line [36]

CHAPTER 3: POWER DIVIDER BACKGROUND

3.1 Scattering Matrix and Properties of Power Divider

It is important to understand scattering matrix as S-parameters are used to characterized the power divider. At higher frequencies, it is hard to measure voltage and current in a circuit. Generally, impedance (Z) matrix and admittance (Y) matrix are used to characterize systems but at higher frequencies, it is difficult to achieve open and short at load, which is required for Z- matrix and Y-matrix analysis, respectively. The open circuit oscillates and the short circuit has some inductance at high frequencies. So, the scattering matrix is used to analyze and characterize systems at microwave frequencies. The scattering matrix is composed of s-parameters, which relates the reflected voltage wave V^- to incident voltage wave V^+. The scattering matrix for N ports can be written as [36] :

$$\begin{bmatrix} V_1^- \\ V_2^- \\ \vdots \\ V_N^- \end{bmatrix} = \begin{bmatrix} S_{11} & S_{12} & \cdots & S_{1N} \\ S_{21} & & & \vdots \\ S_{N1} & \cdots & & S_{NN} \\ \vdots & & & \end{bmatrix} \begin{bmatrix} V_1^+ \\ V_2^+ \\ \vdots \\ V_N^+ \end{bmatrix}$$

(a)

Figure 3.1: Scattering-matrix for N-port network [36]

or

$$[V^-] = [S][V^+] \tag{3.1}$$

The s-parameters can be determined as [36]

$$S_{ij} = \left.\frac{V_i^-}{V_j^+}\right|_{V_k^+=0 \ for \ k\neq j} \tag{3.2}$$

Which means, they can be defined as the ratio of reflected voltage wave from port i to the incident voltage at port j , under the condition that all other ports are match terminated. The match termination means that all ports are loaded with impedance thats is equal to their respective characteristic impedance. As a result, there is no reflection from these ports i.e reflection coefficient $\Gamma = 0$.

Reciprocity of the network also needs to be considered for the analysis of power divider. It is the property of the network, where the magnitude of voltage and current remains the same, even when the ports at which the sources are connected gets interchanged . The impedance and admittance matrices are symmetric for reciprocal network [36]. The scattering matrix is also symmetric as long as the ports are matched at load with their respective characteristic impedances. Reciprocal network with ports having the same characteristic impedance is provided by [36]

$$[S] = [S]^t \tag{3.3}$$

Another property of the network is to determine the loss attribute by it. The impedance and admittance matrix is purely imaginary for lossless network but the scattering matrix given by (3.4) [36], under the condition that characteristic impedance at all ports are same. Thus, scattering matrix for lossless device satisfy

$$[S][S]^{*t} = [U] \tag{3.4}$$

where U is the Identity matrix, the superscript t stands for the transpose of the matrix and superscript asterisk shows the conjugate of the matrix. Scattering parameters calculated only when all ports are in match condition, so these are also called *matched circuit parameters.*

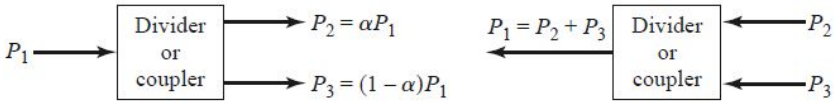

(a)

Figure 3.2: Power divider and combiner model [36]

Figure (3.2) shows a block diagram of power divider. It is a three port network and scattering matrix can be written as [36]

$$S = \begin{bmatrix} S_{11} & S_{12} & S_{13} \\ S_{21} & S_{22} & S_{23} \\ S_{31} & S_{32} & S_{33} \end{bmatrix} \tag{3.5}$$

Ideally, the network should be lossless, reciprocal and matched at all ports, simultaneously. It can be shown by using s-parameters that above mentioned three conditions can't be satisfied for three port network [36]. Considering, first condition that all ports are match terminated. Consequently, $S_{ii} = 0$, which converts the scattering matrix to

$$S = \begin{bmatrix} 0 & S_{12} & S_{13} \\ S_{21} & 0 & S_{23} \\ S_{31} & S_{32} & 0 \end{bmatrix} \tag{3.6}$$

The second condition sates that the network must be reciprocal, which means scattering matrix should be equal to its transpose i.e $S_{ij} = S_{ji}$ according to (3.3), which further reduces the matrix to

$$S = \begin{bmatrix} 0 & S_{12} & S_{13} \\ S_{12} & 0 & S_{23} \\ S_{13} & S_{23} & 0 \end{bmatrix} \tag{3.7}$$

If the network is also considered as lossless then it should satisfy (3.4), according to which [36]

$$|S_{12}|^2 + |S_{13}|^2 = 1 \tag{3.8}$$

$$|S_{12}|^2 + |S_{23}|^2 = 1 \tag{3.9}$$

$$|S_{13}|^2 + |S_{23}|^2 = 1 \tag{3.10}$$

$$S_{13}^* S_{23} = 0 \tag{3.11}$$

$$S_{23}^* S_{12} = 0 \tag{3.12}$$

$$S_{12}^* S_{13} = 0 \tag{3.13}$$

In order to satisfy (3.11-3.13), two of the elements from S_{12}, S_{13} and S_{23} must be equal to zero. Let's assume S_{12}, S_{23} are zero, then equations from (3.11 to 3.13) are satisfied. However, it is evident that equation (3.9) is not satisfied. So, regardless of the two parameters that are chosen from (3.11-3.13), it cannot satisfy all equations from (3.8-3.13). Hence, it is not possible to obtain lossless, reciprocal three port network with all matched ports. Therefore, the power divider is chosen to have lossy network at the same time reciprocal and matched at all ports [36]. The lossy nature of network is used to provide isolation between the output ports ($S_{23} = S_{32} = 0$).

3.2 The Wilkinson Power Divider

Power dividers are generally three port networks. There are commonly three types of power divider used in industry. The first one is T-junction divider which is not matched at all ports and also does not provide isolation between output ports [36]. The second one is resistive divider which suffers from power loss and has less isolation between output ports, even when the ports are matched [36]. The third and most popular one is Wilkinson power divider [37], which was proposed by Ernest Wilkinson in 1960. Figure 3.3 shows the Wilkinson power divider with it's equivalence transmission line circuit.

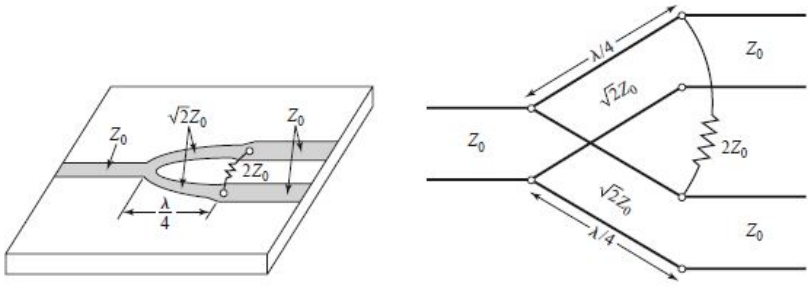

(a)

Figure 3.3: An equal-split Wilkinson power divider with Equivalent transmission line circuit [36]

It can be observed from the Figure 3.3 that a microstrip line which is connected to port 1, splits into two lines which further connects to port 2 and 3. Port 1 is considered as input port while port 2 and 3 are known as output ports. These two splitted lines are of quarter wavelength long at center frequency and have a characteristic impedance of $\sqrt{2}Z_0$, where Z_0 is the characteristic impedance at input port. A resistor of $2Z_0$ is connected between port 2 and 3, at the end of matching section transmission line.

When port 1 is excited and port 2 and 3 are matched, then the power splits in to half with equal magnitude and phase, and comes out from output ports. Due to equal magnitude and phase, the potential difference across the resistor becomes zero. Hence, no power dissipation occurs in the resistor. Similarly, when port 2 and 3 are excited with equal magnitude and phase, when port 1 is match terminated, then also there is no power dissipation in the resistance due to zero potential difference across it. The power from port 2 and 3 gets combined and comes out of port 1. Thus, it also behaves as a power combiner. In other scenario, when only port 2 is excited and port 1 and 3 are match terminated, then half power comes out of port 1 and other half dissipates in resistor. There is no power comes out of port 3, which means it provides isolation between output ports. This condition is also consistent with

reciprocal behavior of the network [37]

The detailed analysis is shown by "even-odd" analysis technique [39].

3.2.1 Even-Odd Mode Analysis

Superposition and circuit symmetry principles are used in even-odd mode analysis. The network design is chosen such that it is symmetric across mid-plane. The characteristic impedance Z_0 at the input port splits into two parallel combination of $2Z_0$, which represents the impedance of matched source. The characteristic impedance of the quater wavelength line is chosen to be $Z = \sqrt{2}Z_0$. The resistor between the output ports divides in two halves as shown in Figure 3.4 Consider a power divider which is matched at all ports and excited at port 2. To simplify the schematics, the ground plane has been removed that includes the bottom conductor of the transmission line. In even-odd mode analysis, the circuit is divided along the plane of symmetry [39]. Consider a Wilkinson power divider that is matched at all ports and excited from port 2 as shown in Figure 3.4

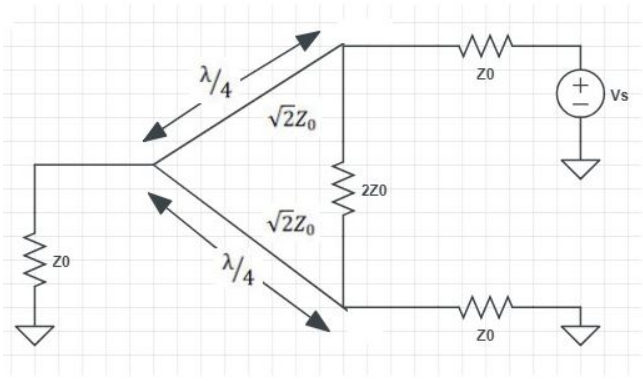

(a)

Figure 3.4: The Wilkinson power divider equivalent circuit excited from port 2

The calculations mentioned below for even-odd mode analysis, comes from the lectures delivered by Dr. Ryan Adams at The University of North Carolina at Charlotte and [36].

3.2.1.1 Even mode analysis

For even mode analysis the circuit can be redrawn as shown in Figure 3.5 with symmetric plane and even excitation.

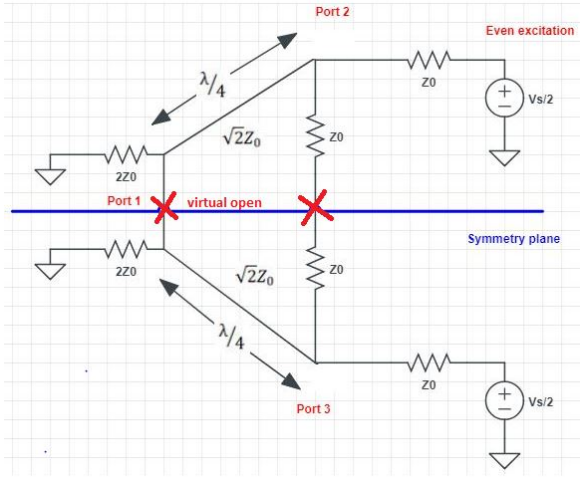

(a)

Figure 3.5: Even mode excitation at output ports

When output ports are excited with sources of equal magnitude and phase then there is a virtual open at the symmetric plane. The isolation resistor does not play any role as there is an open circuit. There is a load of $2Z_0$ at port 1 due to effect of symmetry and open circuit. The circuit in Figure 3.5 is symmetric above and below the plane, so only analysis of half circuit is sufficient. The half circuit after applying even mode conditions reduces to circuit shown figure 3.6:

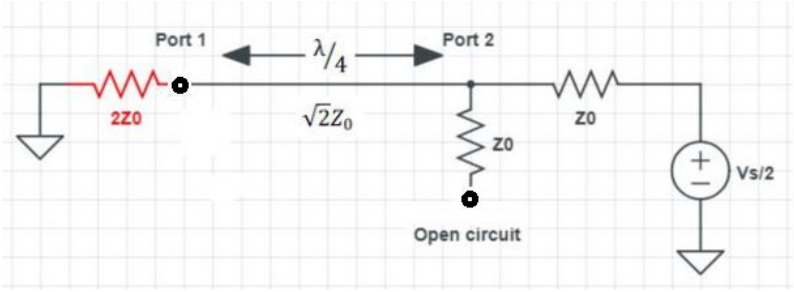

(a)

Figure 3.6: Equivalent circuit at even mode

Input impedance looking in port 2 for even mode Z_{in}^{e} can be given by

$$Z_{in}^{e} = Z_c \frac{Z_L + jZ_c \tan \beta l}{Z_c + jZ_L \tan \beta l} \tag{3.14}$$

Where Z_c is the characteristic impedance of matching section and Z_L is the matched load impedance. By putting the values in 3.14 gives,

$$Z_{in} = \frac{Z_c^2}{Z_L} = \frac{(\sqrt{2}Z_0)^2}{2Z_0} = Z_0 \tag{3.15}$$

it is matched ($Z_{in}^{e} = Z_0$) that means the reflection coefficient at port 2 in even mode is zero $\Gamma_2^e = 0$. Even mode voltage at port 2 (V_2^e) can be determined by voltage division:

$$V_2^e = \frac{V_s}{2} \frac{Z_0}{Z_0 + Z_0} = \frac{V_s}{4} \tag{3.16}$$

Now voltage at port 1 from port 2 in even mode V_1^e needs to be determined, By examining the circuit in figure 3.6

$$V_2^e = \frac{V_s}{4} = V(-\frac{\lambda}{4}) = V_0^+(e^{j\frac{\pi}{2}} + \Gamma_L e^{j\frac{-\pi}{2}}) \tag{3.17}$$

$$V_0^+ = -j\frac{V_s}{4(1-\Gamma_L)} \tag{3.18}$$

where Γ_L is the load reflection coefficient at load $2Z_0$, so value of Γ_L is given by

$$\Gamma_L = \frac{2Z_0 - \sqrt{2}Z_0}{2Z_0 + \sqrt{2}Z_0} = \frac{2-\sqrt{2}}{2+\sqrt{2}} \tag{3.19}$$

If the load is at the origin, i.e $l = 0$, the even mode voltage at port 1 (V_1^e) is ;

$$V_1^e = V(0) = V_0^+(1+\Gamma_L) = -j\frac{V_s}{4}\left(\frac{1+\Gamma_L}{1-\Gamma_L}\right) \tag{3.20}$$

By putting the value of (3.19) in (3.20), the expression simplifies to

$$V_1^e = -j\frac{V_s}{2\sqrt{2}} \tag{3.21}$$

3.2.1.2 Odd mode analysis

In odd mode analysis the circuit is driven at output ports by sources with equal magnitude but opposite phase. This causes a virtual short at the symmetry plane as shown in Figure 3.7

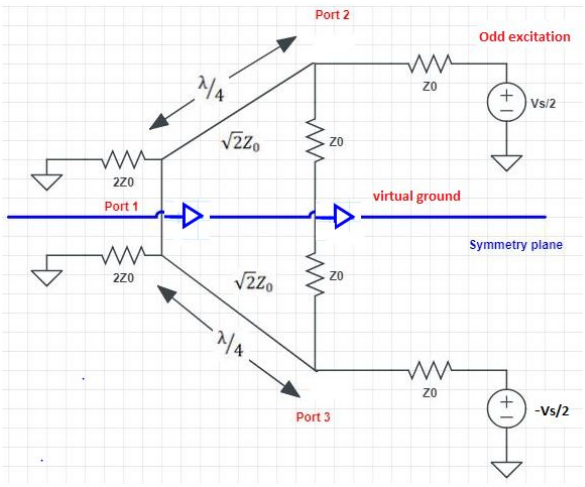

(a)

Figure 3.7: Odd mode excitation at output ports

As a result there is a short circuit at port 1 and the isolation resistor is also shorted to ground. The equivalent half circuit, above the plane of symmetry is shown in Figure 3.8

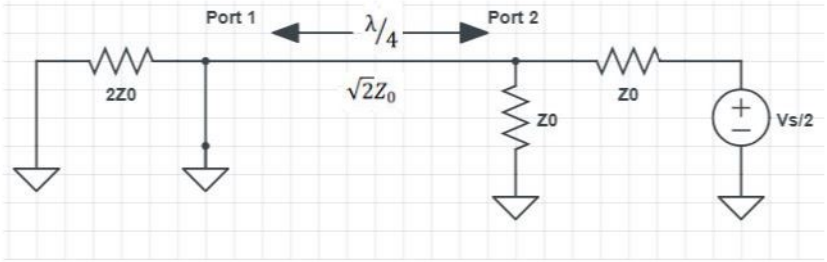

(a)

Figure 3.8: Equivalent half circuit for Odd mode excitation

Analysis on the circuit in Figure 3.8 shows that, the quarter wavelength long transmission line is terminated by shorting the parallel resistor at port 1, where no energy is dissipated in the load at port 1. This results in an odd mode voltage at port 1 (V_1^o) equals to zero. Since the transmission line is quarter wavelength, the input impedance of transmission line looking in from port 2 is given by

$$Z_{in} = Z_c \frac{Z_L + jZ_c \tan \beta l}{Z_c + jZ_L \tan \beta l} \tag{3.22}$$

where Z_L is the load impedance at port 1 which is zero, and the characteristic impedance Z_c is $\sqrt{2}Z_0$. At $\lambda/4$ the expression $\tan \beta l$ goes to infinity, thus by applying L'Hospital's Rule to solve for input impedance seen from port 2:

$$Z_{in} = \frac{Z_c^2}{Z_L} \tag{3.23}$$

As mentioned above the load at port 1 is zero, therefore the equation 3.23 goes to infinity, which can be modeled as open circuit load. Consequently, the reflection coefficient at port 2 in odd mode is zero $\Gamma_2^o = 0$. Hence, it is matched at port 2 in even and odd excitation. The odd mode voltage at port 2can be calculated by applying voltage division.

$$V_2^0 = \frac{V_s}{2}\frac{Z_0}{Z_0 + Z_0} = \frac{V_s}{4} \tag{3.24}$$

When the circuit is excited from port 1, only even symmetry is present as shown in Figure 3.9

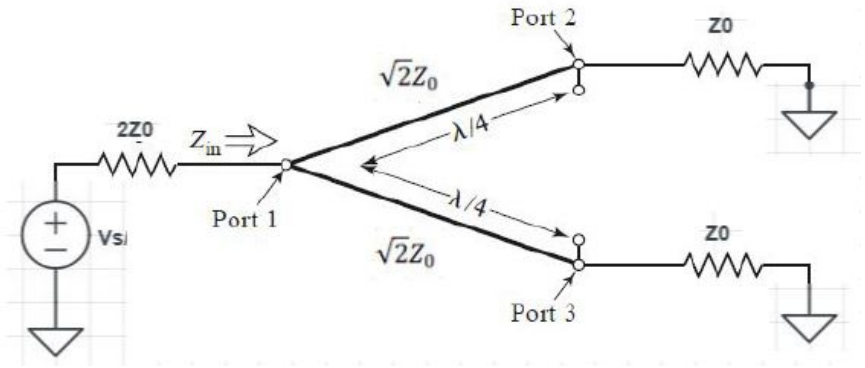

(a)

Figure 3.9: Port 1 excitation even mode equivalent circuit [36]

The input impedance looking into port 1 becomes:

$$Z_{in}^1 = \frac{1}{2}\frac{(\sqrt{2}Z_0)^2}{Z_0} = Z_0 \tag{3.25}$$

Then, the reflection coefficient at port 1 in even symmetry is zero, $\Gamma_1^e = 0$. Thus,

$$S_{11} = 0 \tag{3.26}$$

$$S_{22} = \frac{1}{2}(\Gamma_2^e + \Gamma_2^0) = 0 \tag{3.27}$$

$$S_{33} = \frac{1}{2}(\Gamma_3^e - \Gamma_3^0) = 0 \tag{3.28}$$

So, it is matched at all ports, which further provides

$$V_1^- = V_1^e + V_1^o = -j\frac{V_s}{2\sqrt{2}} \tag{3.29}$$

Outgoing voltage at port 1, when driving at port 2:

$$S_{12} = \frac{V_1^-}{V_{2^+}} = \frac{-j}{\sqrt{2}} \tag{3.30}$$

To measure isolation between port 2 and 3

$$S_{32} = \frac{1}{2}(\Gamma 2^e - \Gamma 2^0) = 0 \tag{3.31}$$

All scattering parameters can be determine by using symmetry and reciprocity, respectively ;

$$S_{13} = S_{12};\ S_{33} = S_{22} = 0;\ S_{23} = S_{32} = 0$$

$$S_{21} = S_{12} = \frac{-j}{\sqrt{2}};\ S_{31} = S_{13} = \frac{-j}{\sqrt{2}}$$

So, the scattering matrix of a Wilkinson power divider is given by:

$$S = \begin{bmatrix} 0 & -j/\sqrt{2} & -j/\sqrt{2} \\ -j/\sqrt{2} & 0 & 0 \\ -j/\sqrt{2} & 0 & 0 \end{bmatrix} \tag{3.32}$$

It is evident from this matrix, that all ports are matched as $S_{11} = S_{22} = S_{33} = 0$. It can also be observed that incident power on port 1 gets equally split between port 2 and 3. When, port 2 and 3 are excited with same magnitude and phase, their power combines and comes out from port 1 without any power dissipation in resistor. On the other hand, when only port 2 or 3 is excited, half of its power goes to port1 and the other half dissipates in the resistor. It also shows,an isolation between port 2 and 3 as $S_{23} = S_{32} = 0$.

3.2.2 Microstrip Design Technique

Microstrip is one of the most popular type of transmission line used today, because of its ease of manufacturing and integration with active and passive device. The geometry is shown in figure 3.10

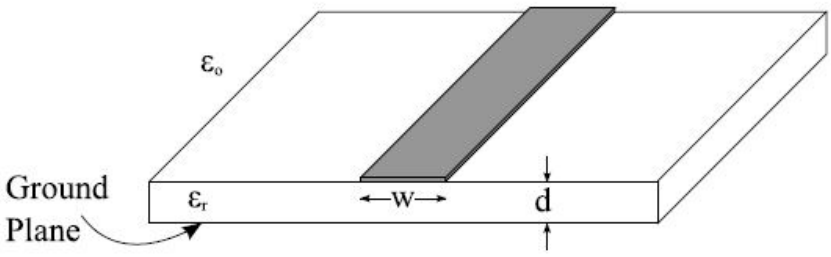

(a)

Figure 3.10: Microstrip structure [36]

Due to the material characteristic of microstrip TEM waves are not strictly supported. As the phase velocities in air and dielectric medium are different. Although an approximation is generated through solution called "Quasi-TEM", under the condition that $d \ll \lambda$. General behavior of the fields within the inhomogeneous medium of microstrip is represented in the figure 3.11 [36] as a rigorous field analysis of this structure is complex

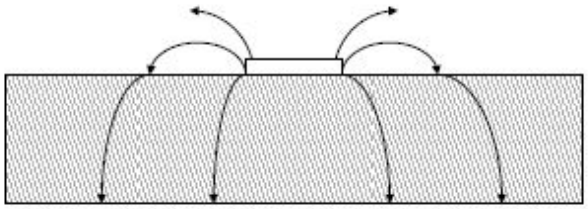

(a)

Figure 3.11: Microstrip fields structure [36].

As part of "Quasi-TEM" approximation the dielectric medium is assumed to be homogeneous by introducing a dielectric constant of ϵ_e, such that $1 < \epsilon_e < \epsilon_r$ [36].

The effective dielectric constant is given by :

$$\epsilon_e = \frac{\epsilon_r + 1}{2} + \frac{\epsilon_r - 1}{2} \frac{1}{\sqrt{1 + 12\frac{d}{w}}} \tag{3.33}$$

The phase velocity and phase constant can be expressed as :

$$\upsilon_p = \frac{1}{\sqrt{\mu_0 \epsilon_0 \epsilon_e}} = \frac{c}{\sqrt{\epsilon_e}} \tag{3.34}$$

$$\beta = \omega\sqrt{\mu_0 \epsilon_0 \epsilon_e} \tag{3.35}$$

where c is the speed of light, d is the thickness of substrate and w is the width of conductor. For a given dimension of a microstrip line, its characteristic impedance is [36]

$$Z_0 = \begin{cases} \frac{60}{\sqrt{\epsilon_e}} \ln(\frac{8d}{w} + \frac{w}{4d}), & \frac{w}{d} < 0 \\ \frac{120\pi}{\sqrt{\epsilon_e}}[\frac{w}{d} + 1.393 + 0.667 \ln(\frac{w}{d} + 1.444)], & \frac{w}{d} > 1 \end{cases} \tag{3.36}$$

These above equations are analysis equations, although designing a microstrip circuit uses the following design equations [36], [40]:

$$\frac{w}{d} = \begin{cases} \frac{8e^A}{e^{2A}-2}, & \frac{w}{d} < 2 \\ \frac{2}{\pi}\{B - 1 - \ln(2B-1) + \frac{\epsilon_r - 1}{2\epsilon_r}[\ln(B-1)) + 0.39 - \frac{0.61}{\epsilon_r}]\}, & \frac{w}{d} > 2 \end{cases} \tag{3.37}$$

where

$$A = \frac{Z_0}{60}\sqrt{\frac{\epsilon_r + 1}{2}} + \frac{\epsilon_r - 1}{\epsilon_r + 1}\left(0.23 + \frac{0.11}{\epsilon_r}\right) \tag{3.38}$$

$$B = \frac{377\pi}{2Z_0\sqrt{\epsilon_r}} \tag{3.39}$$

These equations are based on the work done by Hammerstad [40].

3.2.3 Wilkinson Power Divider Design and Simulation

A single section Wilkinson power divider [37] was designed, to operate at a center frequency of 2 GHz, where ports were matched at 50Ω. Design parameters for this network were characteristic impedance of the input section, the matching section and the load as shown in even-odd mode analysis. The input was 50Ω and the load was

twice as the input i.e 100Ω, for single section power divider [36]. The characteristic impedance of matching section was found by taking the square root of the product of the input characteristic impedance and the load characteristic impedance [36]. The characteristic impedance of matching section was given by

$$Z_1 = \sqrt{Z_o Z_L} = \sqrt{50 \times 100} = 70.7\Omega$$

The board material used for the design of power divider was FR-4 that has a relative permittivity of 4.4. The thickness of the substrate used was 1.6 mm and the thickness of the conductor was 0.035 mm. Equations (3.37 - 3.39) were used, to find the dimensions i.e width and length of the microstrip. It was observed that the thickness of the substrate plays a crucial role in determining the width of the microstrip. The width of the microstrip determines are characteristic impedance and was inversely proportional to the characteristic impedance. Since, the length of a microstrip was quarter wavelength long and it was a strong function of effective permittivity, because the wavelength depends on the effective permittivity. In order, to provide isolation between the output ports, 100Ω lumped resistance was used between port 2 and 3. The table mentioned below showed the dimensions of power divider.

Table 3.1: Dimensions of Wilkinson power divider.

Characteristic Impedance	Width (mm)	Length (mm)
50Ω	3.059	20.55
70.7Ω	1.6215	21.04

The design was laid out in HFSS (High Frequency structure Simulator) which was a 3D electromagnetic simulator for high frequency electronic circuits. HFSS used finite element method solver for electromagnetic structures. The design of a power divider was shown in the figure 3.12

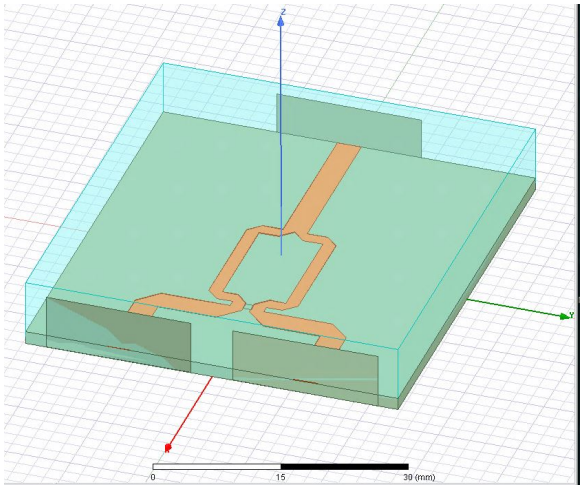

(a)

Figure 3.12: Wilkinson power divider design in HFSS.

The inner edges were designed to be quarter wavelength, to get the optimum response. It was observed that energy cut corners so, chamfers were used to get desired frequency response. The S-parameter results after simulation were shown in the figure 3.13. As expected, at 2GHz return loss S_{11} was 35dB which was consistent with calculated parameters. The reflection coefficient S_{11} was below -10dB from 1 GHz to 3 GHz which was the operating bandwidth of power divider and the pattern continues till 7 GHz, due to higher order harmonics.

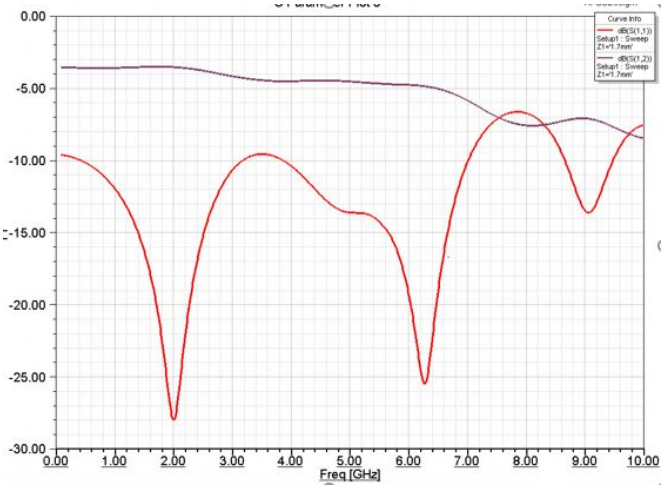

(a)

Figure 3.13: Return loss S_{11} and transmission loss S_{21} at port 1

Similarly, equal power division i.e -3dB split was verified by observing the transmission loss (S_{21}) in Figure 3.13. The S_{21} is close to -3dB across the band. It was also observed that S_{21} reduced at higher frequencies. The decrease in the transmission loss was due to the increase in dielectric losses at higher frequencies. Major contribution to the lossy behavior is due to the changes in dielectric constant of FR4 at higher frequencies. The circuit was fabricated and measured results were in good agreement with simulated results as shown in Figure 3.14 and Figure 3.15

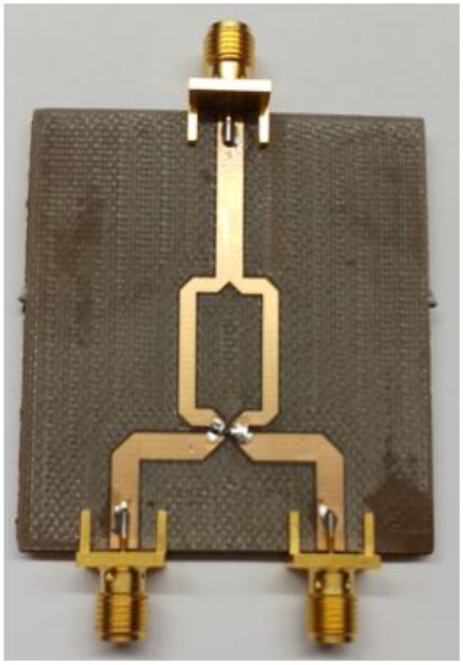

(a)

Figure 3.14: Fabricated design of power divider

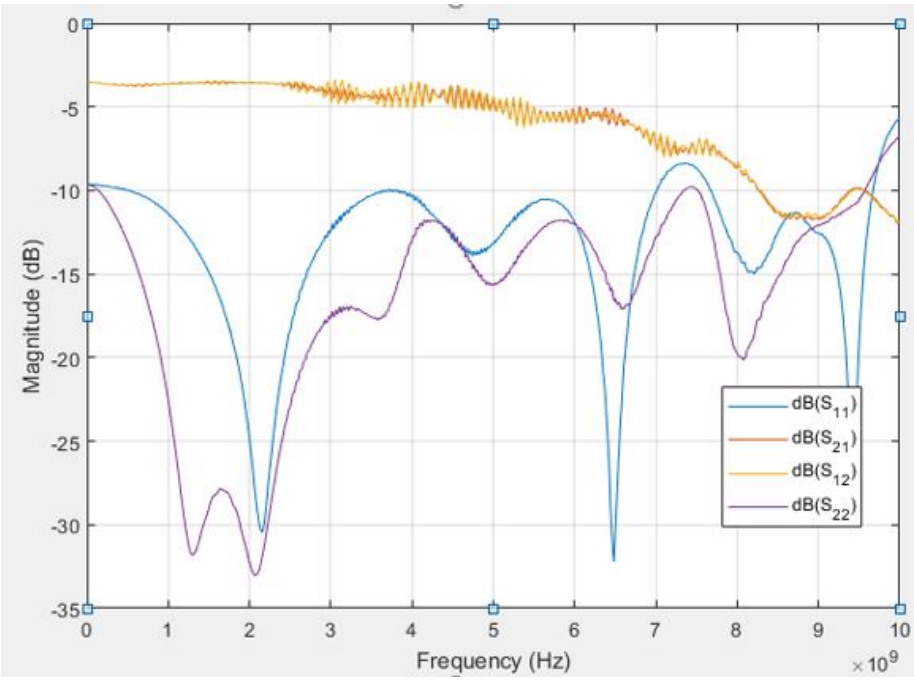

(a)

Figure 3.15: Measured S_{11} and S_{21} at port 1

CHAPTER 4: DEFECTED SIGNAL LINE STRUCTURES

4.1 Background of Defected Structures

The Photonics bandgap structures which are periodic in nature, have a property where the optical waves cannot propagate in certain frequency bands [46],[47]. It was shown in late 1980's that, due to the analogous nature of electromagnetic wave propagation in multi-dimension periodic structure and propagation of electron waves in crystal. It was expected to achieve same bandstop frequency response for electromagnetic waves. Yablonovitch introduced Electromagnetic bandgap structures which were equivalent to photonics bandgap structures [41],[42]. These structure have huge application in millimeter wave and microwave circuit design[43] - [45].

These periodic structures can be designed by etching the metal from ground plane [4] , distorting the signal line structure [48] or by drilling holes in form of square , triangular or honeycomb lattice in the substrate [3]. The advantages of these structures are, first that these periodic structures does not allow electromagnetic waves to propagate in certain frequency bands. This property provides bandstop filtering response, which also suppress higher order harmonics [13]. The second important property is that the effective inductance and effective capacitance of the line increases due to the presence of these periodic structures, which in turns increase the characteristic impedance of the transmission line. This property is used in reducing the size of the device [13]. The third property is that due to their presence circuit has better transmission loss and return loss because of their ability to suppress the surface wave. The multiple reflection between the ground plane and air-dielectric interface are the cause of electromagnetic surface wave [13]. These structures are easy to fabricate, economical and compatible with standard technology used in circuit design. They

are widely used in designing filters, antenna,amplifier, wave guide and others [49]-[52] .

The biggest disadvantage of EBG structure is the complexity in modeling these structures. There are so many parameters that needs to be considered like shape , size, location and lattice period. The other issue is the full wave simulation of these structures take a very long time. Due to such problems, defected ground structures were evolved. DGS are unit cell resonating structures which are created by etching metal from ground plane. These are not periodic structures, only unit cell is sufficient to achieve bandstop frequency response. They have all the properties offered by EBG structure and also they are very simple to model [54]. Because of such interesting properties, there is so much research going in this area to find compact DGS to reduce size of circuits . Defected structure in signal line is an extension and further evolution of defected structures that can be evaluated and modeled similar to DGS. Another disadvantage of DGS is they can work only in standalone environment, where customizing the ground plane can also affect the frequency response of other components in RF circuits. On the other hand DSS can operate in a group, where slots in one trace will not impact the other. DSS structures will play crucial role in the designing circuits for millimeter wave range.

4.1.1 Equivalent Circuit of Defected Signal-line Structure

The method used to find the equivalent circuit model and to extract it's parameters is based on electromagnetic simulations. A full wave Electromagnetic solver like HFSS is used to extract s-parameters vs frequency for a single DSS unit cell. The simulated results are used to analyze the cutoff and resonance frequency of DSS. Once the S-parameter vs frequency graph is obtained, various combinations of RLC are modeled, depending on the frequency response. The parameters of the equivalent circuit can be extracted by equating simulation results to single section bandstop filter. This method is simple, compared to conventional methods but it doesn't give any insight

about the working of DSS. There is no direct correlation between the dimensions of DSS and it's equivalent circuit. The following flow chart in figure 4.1, shows the conventional design and analysis of DSS [53], [54] .

Generally, there are three types of equivalent circuits : (1) LC and RLC equivalent circuit (2) π shaped equivalent circuit, (3)quasi-static equivalent circuit.

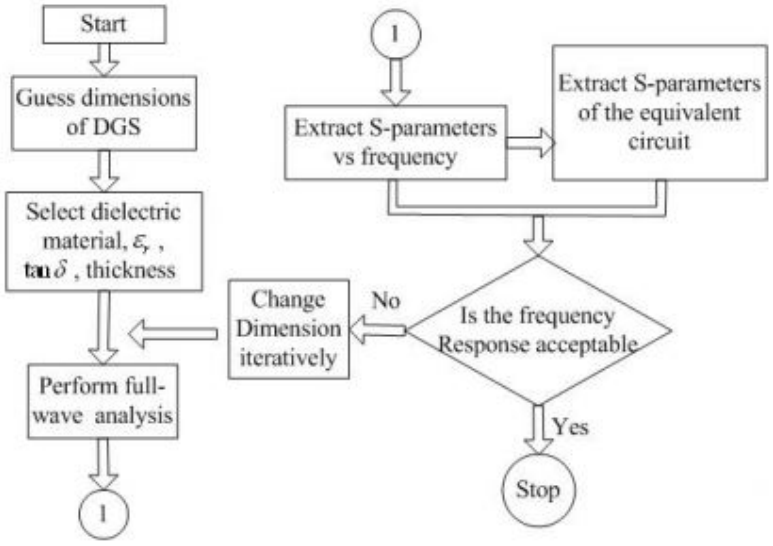

(a)

Figure 4.1: . Conventional design and analysis method [53]

LC and RLC equivalent circuits

The equivalent circuit of a DSS can be modeled as shown in figure 4.2, as a bandstop filter. The DSS increases the route length of the current due to which the effective inductance increases. The slot gap is responsible for the effective capacitance of the microstrip line, hence this structure can be modeled as a combination of inductance and capacitance in parallel. DSS has certain resonating frequency and can be observed in s-parameter results from EM simulation. Therefore, the equivalent circuit has a pair of parallel inductor-capacitor in it. It was also observed, that as the length of the etched area of the slot increases, the effective inductance increases with it,resulting in a lower resonance frequency. Effective Capacitance depends on the coupling and the

coupling increases with tighter gap. Hence more effective capacitance can be achieved by making small gap structure and vice versa [54],[55].

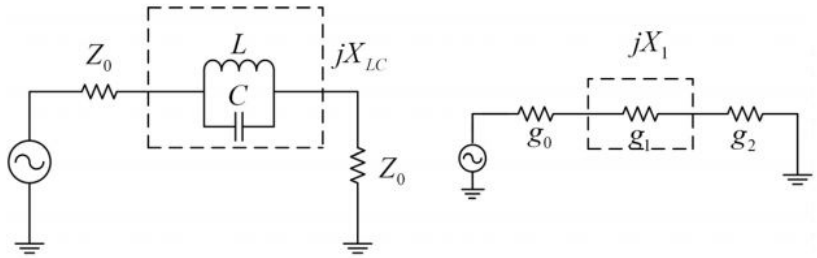

(a)

Figure 4.2: . LC equivalent circuit for DSS [55]

Simulated results of DSS are used to extract the parameters, for equivalent circuit of DSS. The simulated results can be equated to a single section bandstop filter [54],[55]. The prototype elements value of bandstop filter given in various sources [56], is used to calculate the series reactance value, shown in Figure 4.2. The resonance frequency extracted from simulation is used to calculate the parallel capacitance value of DSS unit cell. To equate DSS to bandstop filter the reactance value of both circuits are equal at cutoff frequency . So, L and C derived as follows [54],[55]:

$$X_{LC} = \frac{1}{\omega_0 C}\left(\frac{\omega_0}{\omega} - \frac{\omega}{\omega_0}\right) \tag{4.1}$$

where, ω_0 is the resonance angular frequency of the parallel LC resonator.

$$C = \frac{\omega_c}{Z_0 g_1} \cdot \frac{1}{\omega_0^2 - \omega_c^2} \tag{4.2}$$

$$L = \frac{1}{4\pi^2 f_0^2 C} \tag{4.3}$$

where f_0 and f_c are the resonance frequency and cutoff frequency, which can be obtain by EM simulation. Therefore, each equivalent-circuit parameters can be obtained by using (4.2) and (4.3).The other DSS structures modeled as low pass or bandstop filter have similar characteristics, although the radiation effects are neglected. The most general and efficient way to model DSS is by parallel $R, L, andC$ resonating structure

connected to transmission line at both sides, as shown in figure 4.3. The resistance is accounting for radiation, dielectric and conductor losses. The equivalent R, L and C values are obtained from the expression [53],[57],

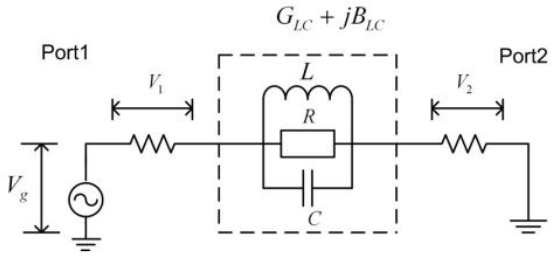

(a)

Figure 4.3: . RLC equivalent circuit for unit DSS [53],[57].

$$\begin{cases} C = \frac{\omega_c}{2Z_0(\omega_0^2 - \omega_c^2)} \\ L = \frac{1}{4\pi^2 f_0^2 C} \\ R(\omega) = \frac{2Z_0}{\sqrt{\frac{1}{|S_{11}(\omega)|^2} - (2Z_0(\omega C - \frac{1}{\omega L}))^2 - 1}} \end{cases} \tag{4.4}$$

4.1.1.1 π shaped equivalent circuits

The suppression of harmonics requires achieving bandpass and bandstop response, simultaneously. This characteristics is challenging for DGS implementation. π model is considered to provide more accuracy compared to LC and RLC equivalent circuits. The figure mentioned below shows the π shaped model [58], [53]

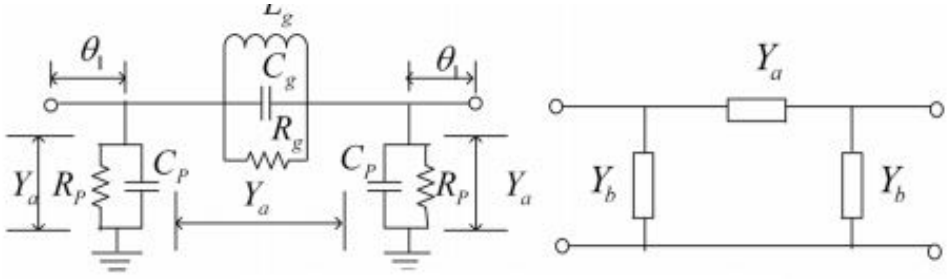

(a)

Figure 4.4: . π shaped equivalent circuit for unit DSS [58], [53].

In order to achieve detailed results, Park[58] proposed π model that shows both amplitude and phase vs frequency response, but it makes the circuit more complex. As a result,extraction of equivalent circuit parameters are difficult. The ABCD parameters of the unit cell can be obtained by using following expressions [58], [53]:

$$\begin{bmatrix} A & B \\ C & D \end{bmatrix} = \begin{bmatrix} 1+\frac{Y_b}{Y_a} & \frac{1}{Y_a} \\ 2Y_b+\frac{Y_b^2}{Y_a} & 1+\frac{Y_b}{Ya} \end{bmatrix} \tag{4.5}$$

$$\begin{cases} Y_a = \frac{1}{R_g} + jB_r \\ Y_b = \frac{1}{R_p} + jB_p \\ C_g = \frac{B_r}{\omega_2(\frac{\omega_1}{\omega_2}-\frac{\omega_2}{\omega_1})}, L_g = \frac{1}{\omega_2^2 C_g}, C_p = \frac{B_p}{\omega_1} \end{cases} \tag{4.6}$$

It is challenging to perform full wave analysis, and it does not provide any physical insight on the working principle of DSS.

4.1.1.2 Quasi-static equivalent circuit

Quasi-static equivalent circuit analysis follows the derivation from the physical dimensions of the DSS, different from of equivalent circuits mentioned above. The figure shows the Quasi- static model for dumbbell shaped structure [53], [59]

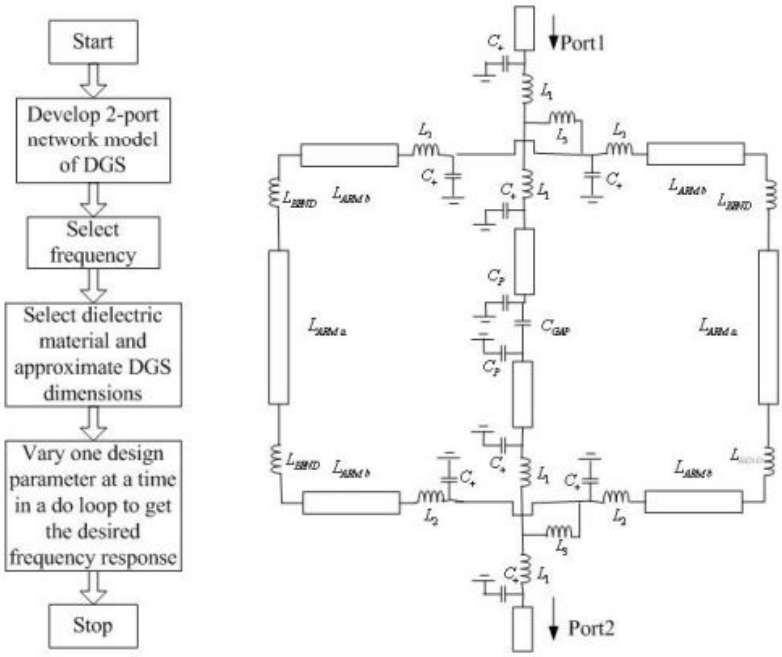

(a)

Figure 4.5: . Quasi static design and analysis method of DSS [53], [59]

This provides a very comprehensive analysis of the structure by breaking the structure into its small physical dimensions and analyzing the effect of individual one. The overall bandpass or bandstop response is dependent on these small physical dimensions, where the type of response can be determined from the dimensions. It eliminates the requirement of doing a full wave analysis by developing equivalence circuit. Currently, there is no uniform circuit model that supports the mathematical theory of the analysis of DSS, as there are different structures with different corresponding properties. Thus optimization based on equivalence circuit model is highly desirable to design this kind of circuit configuration .

4.1.2 Defected signal-line U-slot Structure

Woo and Lee [60] discussed U-slot DGS for bandstop filter with improved Q factor,in a great details. They proposed U-slot to achieve narrow band bandstop response, even with it's simple structure. It was also proved that Q factor was inversely

proportional to slot width g. In this document, the characteristics of U-slot etched on signal line was analyzed. The method for analysis of defected signal line(DSS) was similar to defected ground structure(DGS). There were two reasons for choosing this structure compared to other DSS, first one was that it provided a steep band-stop frequency response as compared to other defected structures like dumbbell and spiral-shaped defects. Hence, due to narrow bandstop response,the undesired signals which were near to the required spectrum can be filtered. The second reason was the dimension of DSS, the longer slots of U-slot were along the transmission line, which was required to integrate it with Wilkinson power divider.

Figure 4.6 showed the etched U-slot on the signal line trace.

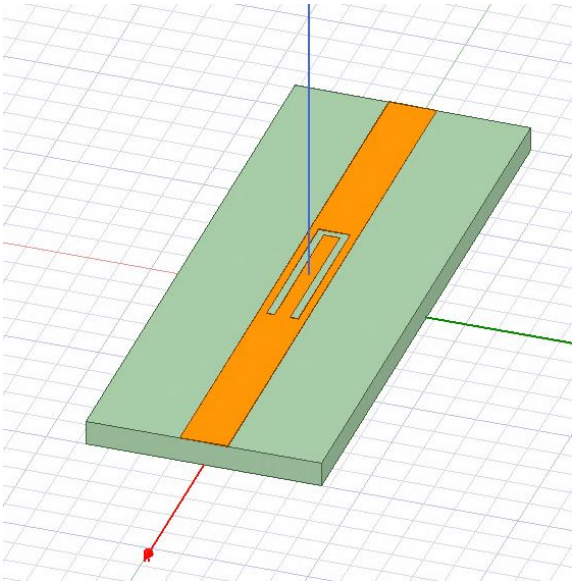

(a)

Figure 4.6: Microstrip line with U-slot DSS

It was shown in Figure 4.6, that two slots of length l along the microstrip line were etched from signal line. The width of these slots were represented by g and distance between them was d. They were connected from one end with slot of width c [60]. The transfer characteristics for these dimensions of U-slot $l = 10.0mm$,$c = g = 0.5mm$ and $d = 1mm$, were calculated in this section. The characteristic impedance of

microstrip line was 50Ω and the simulation was performed by using HFSS. The FR4 board with substrate thickness of 1.6 mm and dielectric constant of 4.4 was used for simulation. The width of the microstrip was calculated by using (3.37) equations, to be 3.059 mm. Figure 4.7, showed the simulated results of S-parameters S_{11} and S_{12} as a function of signal frequency. The designed U-slot DSS provided the band rejection property of 18dB at 4.4 GHz(3-dB bandwidth of 1.02 GHz). The Q factor of the proposed U-slot DGS was 3.9.

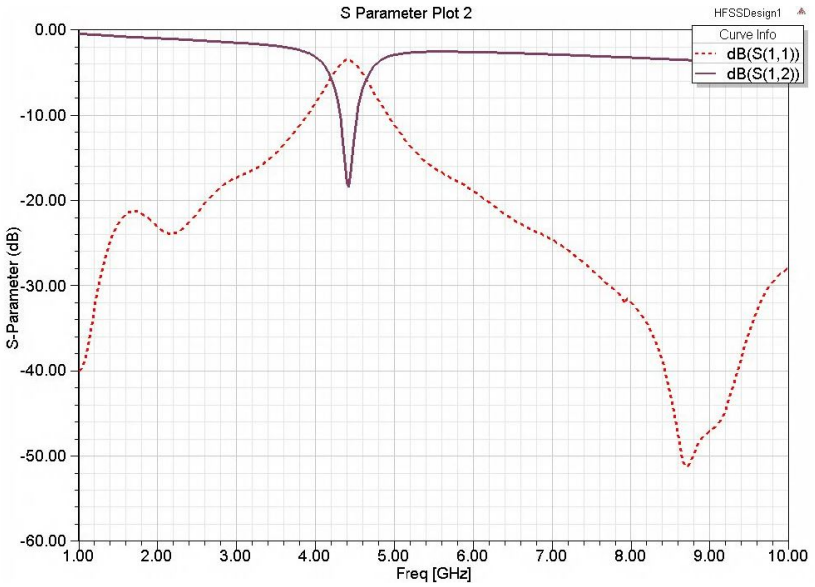

(a)

Figure 4.7: Transfer characteristics of U-slot DGS (l = 10.0 mm,c = 0.2 mm,g = 0.5 mm,d = 1.0 mm, " of substrate = 4.4, thickness of substrate = 1.6 mm)

4.1.2.1 Modeling and Parameter Extraction

The previous section showed that U-slot DSS could be modeled as parallel LC resonance circuit, which blocked the signal at frequency of resonance. In order to extract the equivalence parameters from DSS, the procedure mentioned below was followed . After simulating the structure shown in figure [4.6], the resonating frequency and 3 dB cutoff bandwidth of the circuit was extracted from S-parameters (S_{11} and S_{12}). After putting resonating frequency and 3 dB cutoff bandwidth in equation [54] men-

tioned below, values of equivalent parameters were calculated to be C = 1.67pF and L = 0.78nH.

$$C = \frac{\omega_c}{2Z_0(\omega_0^2 - \omega_c^2)}; L = \frac{1}{4\pi^2 f_0^2 C}$$

The plot in figure 4.8 showed an agreement between calculated equivalent circuit parameter with field calculated results, that proved the validity of the circuit parameters for circuit design.

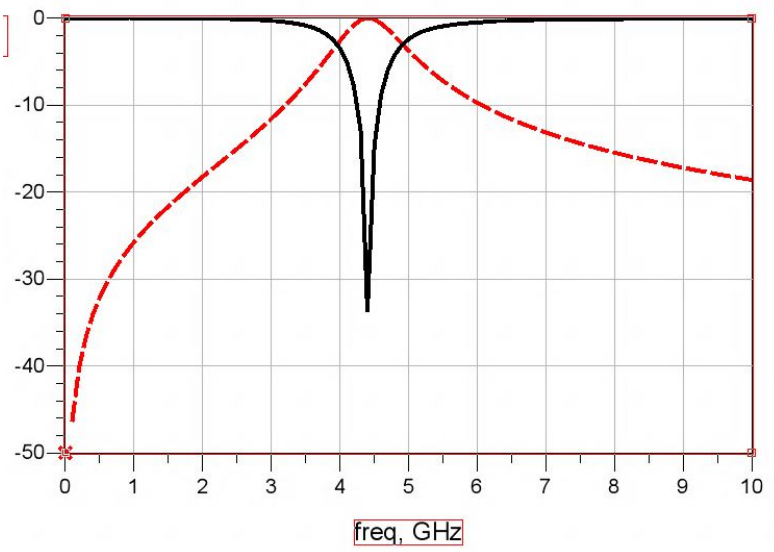

(a)

Figure 4.8: Extracted LC parameter of DSS

4.1.2.2 Influence of Length of Structure

Again 50 Ω microstrip line was used for all simulations. The simulated transfer characteristic of U-slot DSS was shown in figure 4.9. Four U-slot DSS were plotted with different dimensions. The length of U-slot was varied and the width of slot g, slot c and distance between two slots d was kept constant.Again, same substrate thickness of 1.6 mm and dielectric constant of 4.4 was used for all simulations.It was clear from the results shown in figure 4.9, that series inductance was directly proportional to the length of the U-slot DSS. As shown in the Figure 4.9, that when length was

increasing from 9 mm to 20 mm, the inductance increased from 0.7 nH to 1.2 nH. It can also be observed that, the resonating frequency reduced from 6.57 GHz to 3.92 GHz as the length increased. The capacitance was also increasing along with the length. Hence, bandstop response can be achieved at any frequency, by just changing the length of the U-slot DSS.The presence of attenuation pole was illustrated in the simulated result and was responsible for the capacitance, in parallel with inductance. The capacitance was due to the coupling within the slot width g. The above results were also supported by the data in Table 4.1. The dimension of U-slot DSS were $d = 1.0$ mm and $c = g = 0.5$ mm. As the slot length increased, both the equivalent capacitance and equivalent inductance increased as shown in the calculated data in Table 4.1. The change in calculated Q factor was observed to be very small as the slot length varies.

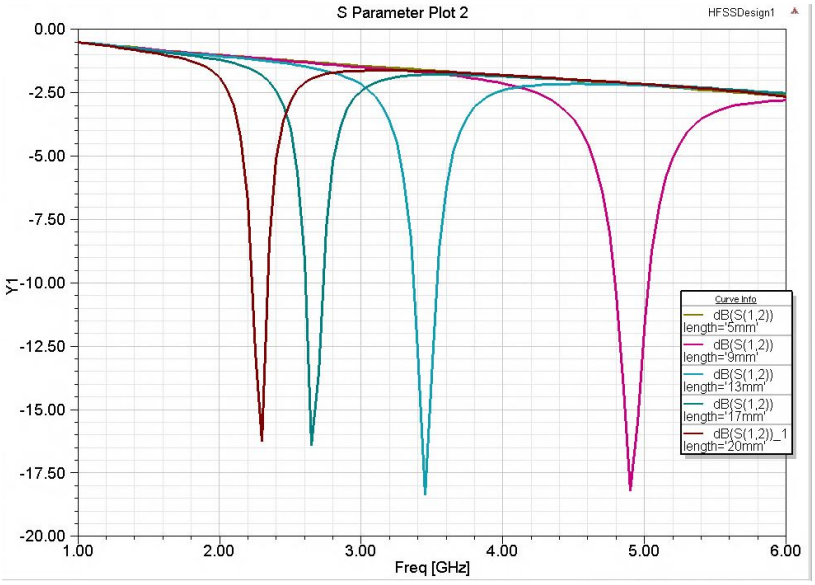

(a)

Figure 4.9: Transfer characteristics for changes in slot length

Table 4.1: Equivalent circuit parameters for changes in slot length.

Length l (mm)	Resonance Frequency (GHz)	Cutoff Frequency (GHz)	3dB Bandwidth (GHz)	Q-Factor	Capacitance (pF)	Inductance (nH)
9 mm	4.9	4.4	1.25	3.92	1.5	0.7
13 mm	3.45	3.15	0.65	5.3	2.53	0.84
17 mm	2.65	2.45	0.45	5.88	3.82	0.94
20 mm	2.3	2.1	0.35	6.57	3.79	1.2

4.1.2.3 Influence of slot width

In the analysis, the length of the slot was kept constant and width of the slot was varied. As expected, due to constant length, the inductance remained constant. Hence,a very small variation in resonance frequency. This showed, that series inductance was independent of width of slot. It was evident from the figure 4.10, that the attenuation pole location was varying with respect to change in width of slot. The width was inversely proportional to effective capacitance, so as the effective capacitance decreases, the attenuation pole location moves up to higher frequency. The simulated transfer characteristics for various slot width were shown in Figure 4.10. The dimensions of the U-slot DSS were $l = 10.0mm$, $d = 1.0mm$. As the slot width increased, the equivalent capacitance decreases and the equivalent inductance increases; the resonance frequency slowly decreases due to the inductance increases. In Table 4.2, it was confirmed that the calculated Q factor increased as the slot width decreased and vice versa.

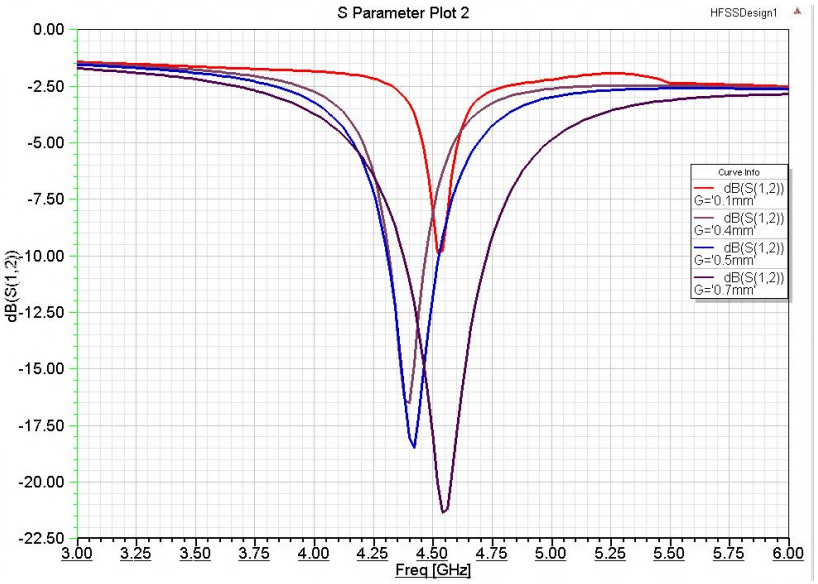

(a)

Figure 4.10: Transfer characteristics for changes in slot Width

Table 4.2: Equivalent circuit parameters for changes in slot width

Width(w)mm	Resonance Frequency (GHz)	Cutoff Frequency (GHz)	3dB Bandwidth (GHz)	Q-Factor	Capacitance (pF)	Inductance (nH)
0.1	4.52	4.38	0.32	14.125	5.5	0.22
0.4	4.4	4.04	0.8	5.5	2.11	0.6
0.5	4.42	3.96	1.04	4.25	1.6	0.79
0.7	4.55	3.84	1.82	2.5	1.02	1.19

4.1.2.4 Influence due to distance between two slots of structure

Figure 4.11 showed the simulated transfer characteristics as a functions of distance between two slots d and the extracted equivalent-circuit parameters and calculated factors were given in Table 4.3. The key observation was that as the distance becomes small the effective capacitance increases due to which the frequency response become more narrow and steep. This steepness increased the Q factor [60]. This can be

clearly observed from Table 4.3.

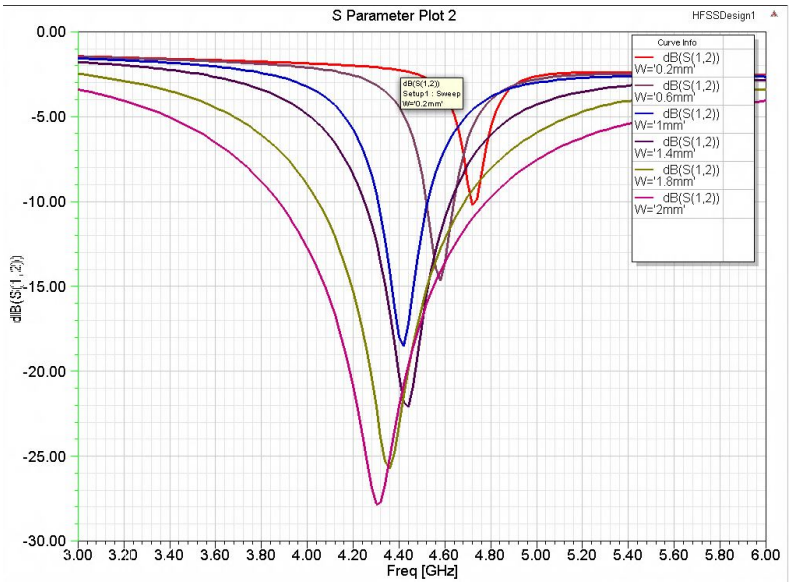

(a)

Figure 4.11: Transfer characteristics for change distance between the slot

Table 4.3: Equivalent circuit parameters for change distance between the slot

Distance(d)mm	Resonance Frequency (GHz)	Cutoff Frequency (GHz)	3dB Bandwidth (GHz)	Q-Factor	Capacitance (pF)	Inductance (nH)
0.2	4.72	4.56	0.36	13.1	4.88	0.23
0.6	4.58	4.28	0.66	6.93	2.56	0.47
1.4	4.44	3.74	1.86	2.38	1.03	1.23
2	4.3	2.84	5.14	0.8	0.433	3.15

4.1.3 Novel G-slot Defected Signal-line Structure

The design of the proposed G-slot DSS was shown in figure 4.12. Similar methodology, like U-slot DSS was used for analysis and parameter extraction. The advantage of this structure over U-slot DSS was the compact structure, which provided more inductance and capacitance to resonate at lower frequency and it also provided more

narrow bandstop response as shown in Figure 4.13. The dimensions of this structure were defined as gap g which was the width of etched surface was kept common and distance between the adjacent slot was w and length of each slot was l. This structure was drawn on 3.059 mm wide, 50Ω microstrip line. The dimension of the structure were, length $l = 10$ mm, gap $g = 0.4$ mm and distance between the slot $w = 3$ mm.

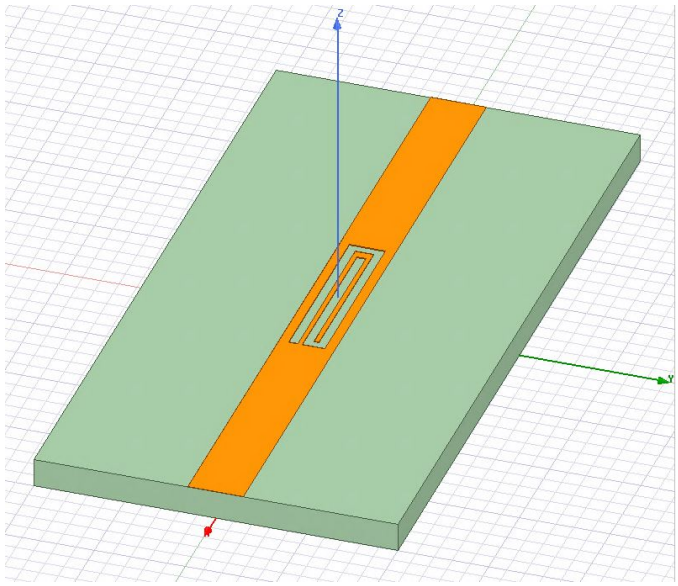

(a)

Figure 4.12: G-slot structure

Transfer characteristic of G-slot was plotted in Figure 4.13 and variation of slot length, width and distance between slot was plotted in Figure 4.14,4.15,4.16 respectively. Figure 4.14 confirmed the presence of high inductance as, it resonated at lower frequency compared to U-slot DSS of same length. It was also depicted in Figure 4.17 that G-slot provided multiband response.

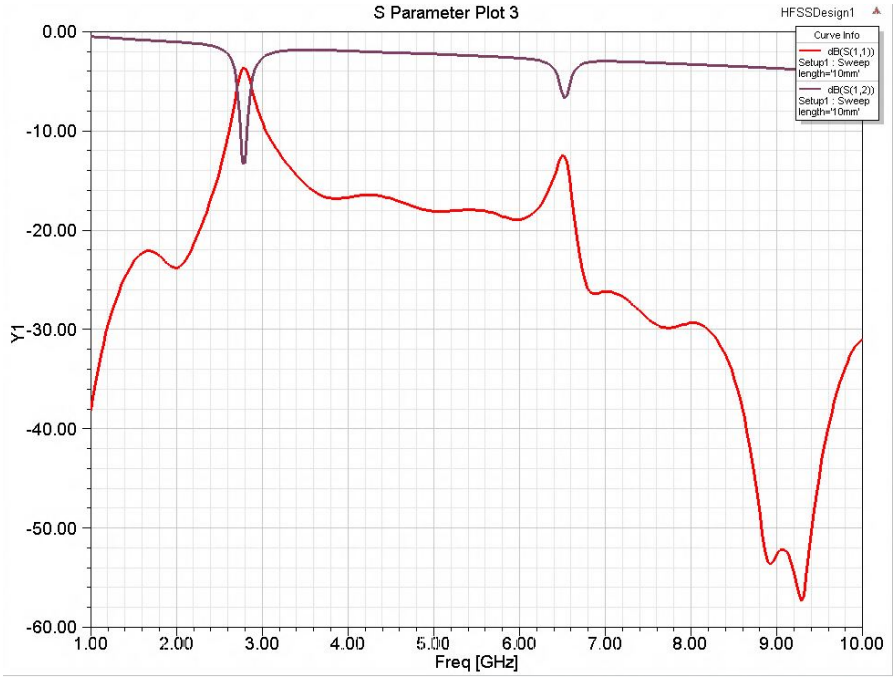

(a)

Figure 4.13: Transfer characteristics of G-slot structure

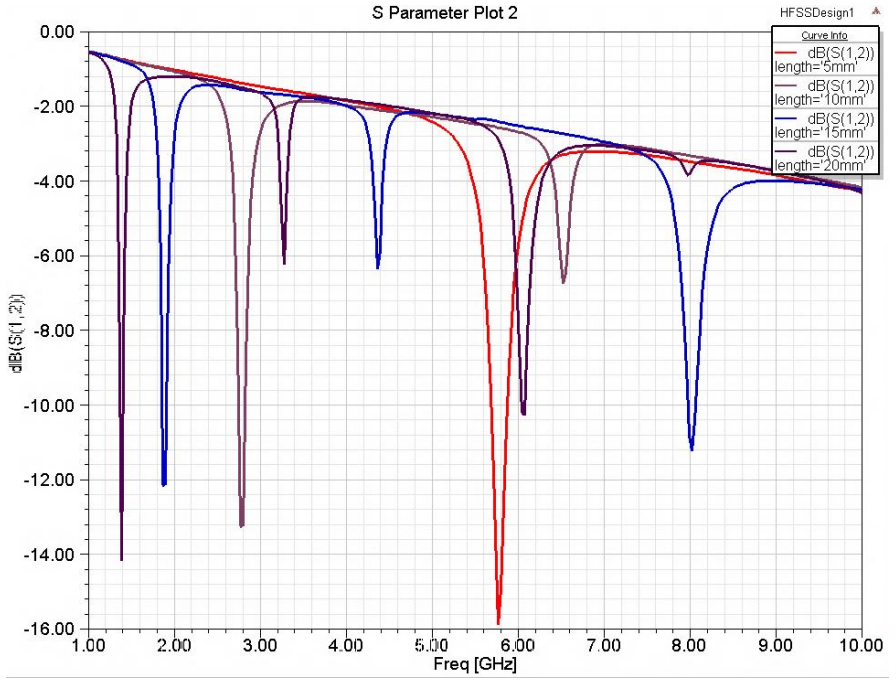

(a)

Figure 4.14: Transfer characteristics for changes in slot length and multiband

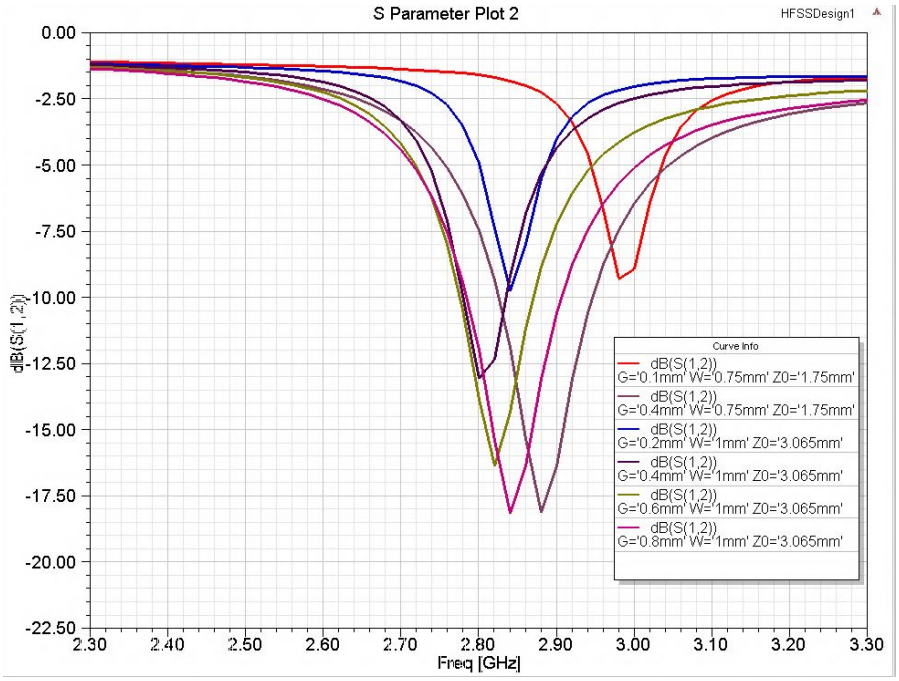

(a)

Figure 4.15: Transfer characteristics for changes in slot Gap

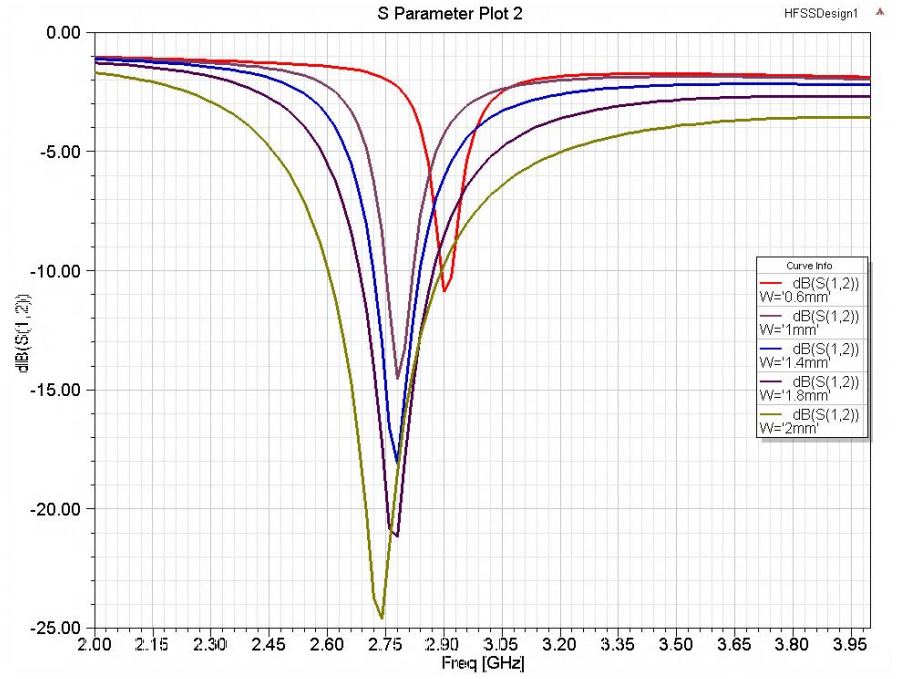

(a)

Figure 4.16: Transfer characteristics for change distance between the slot

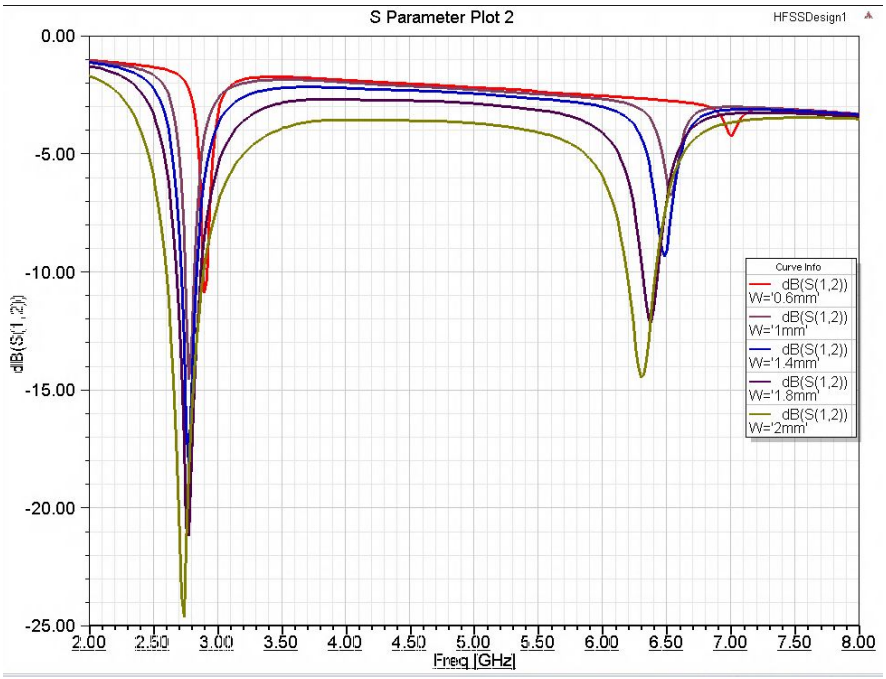

(a)

Figure 4.17: Multiband response

CHAPTER 5: POWER DIVIDER WITH DEFECTED SIGNAL-LINE

The objective of this section was to investigate the application of various defected signal line structures integrated with a single section Wilkinson power divider. Through this investigation, it was observed that properties like bandstop filtering and tunable multi-band responses can be achieved by combining these two structures. Furthermore, the slots etched from the signal line of the power divider did not require any additional space in the circuit board, eliminating the need for a separate filter circuit, and reducing the overall size of the circuit. Each simulation was performed using Ansys HFSS, FR4 board with a dielectric constant of 4.4 and a height of 1.6 mm was used to simulate and fabricate all of the structures. The following section describes each applications:

5.0.1 Bandstop Response

Bandstop application gives a notch filter response to stop interference in the adjacent band. A G-slot defected signal line structure provided a sharp bandstop response as shown in the previous section. The motivation for choosing this structure was to have a resonance at a lower frequency within the limited dimensions of the Wilkinson power divider's arm. Likewise, the G-slot DSS provided more effective inductance and capacitance in the same area compared to the U-slot DSS, which produce resonance at lower frequencies.

A single section Wilkinson power divider was designed at a center frequency of 2 GHz. The dimensions of the 50 Ω transmission line in the power divider were $l = 20.44$ mm long and $w = 3.059$ mm wide respectively. While the matching section of the power divider with a characteristic impedance of 70.7 Ω has length of $l = 21.45$ mm and a

width of $w = 1.672$ mm however for this structure the width was set to be 1.9 mm to achieve a reasonable gap for milling the structure. This increase in width reduces the characteristic impedance, but has very little impact on the simulated results. The length of the G-slot, along the length of power divider's arm was $l_s = 11.5$ mm. The distance between the slots was $w = 0.25$ mm and the etched gap was $g = 0.3$ mm. Figure 5.1 and Figure 5.2 shows the circuit design and the S-parameters, S_{11} and S_{12} for the G-shaped DSS.

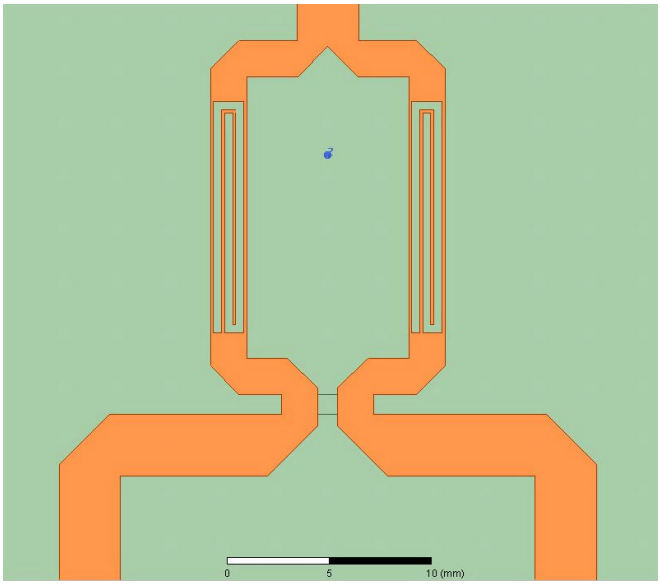

(a)

Figure 5.1: G-Slot DSS integrated with power divider

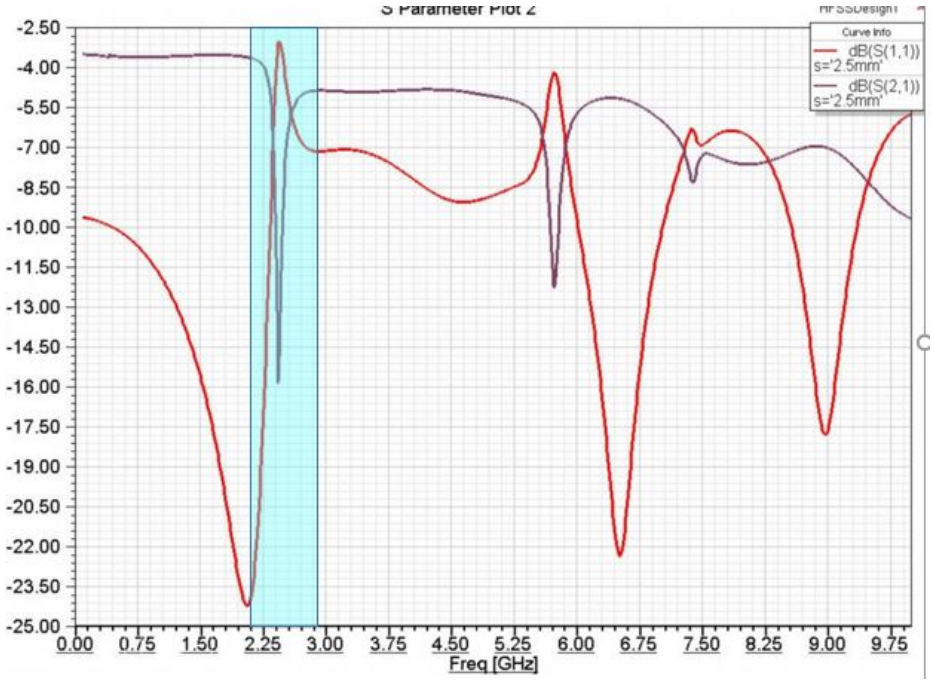

(a)

Figure 5.2: S-parameters for G-slot integrated with power divider

Figure 5.1 and Figure 5.2 illustrate that integrating DSS with power divider produced a bandstop response at 2.4 GHz, where insertion loss S_{12} reduced to -16 dB. The power divider operated from 250 MHz to 2.25 GHz frequency band, as the return loss (S_{11}) was below -10dB, and transmission loss was around 3.5 dB in this frequency range. There is a notch at 2.4 GHz, due to the resonance provided by DSS, showing that much less energy was transmitted at this frequency. As shown from Figure 5.2 that its a narrow band response. The dimensions of defected structure were responsible for the frequency where resonance occurs. The narrow bandstop response can be achieved at any desired frequency simply by changing the dimensions. Figure 5.3 and 5.4 showed the fabricated circuit and measured data, they were in agreement with the simulated results.

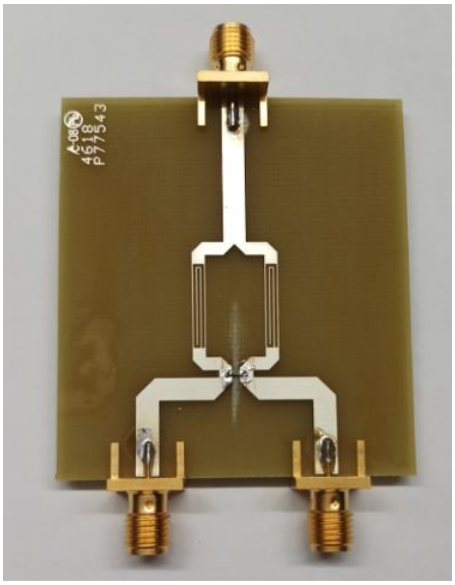

(a)

Figure 5.3: Fabricated G-Slot DSS integrated with power divider

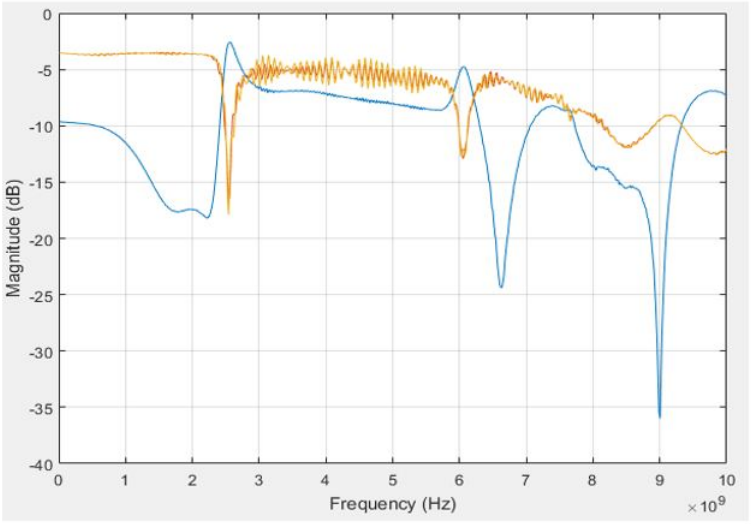

(a)

Figure 5.4: Measured S-parameters for G-slot integrated with power divider

5.0.2 Multi-band Response

Figure 5.3 shows the design of the power divider with the slot etched till the end of the arm. This type of design forces energy into small traces due to which effective

inductance and capacitance further increases,giving it a narrow band response at lower frequency, as well as resonance at other frequencies. In sum, by customizing the dimensions of a defected signal line structure, multi-band response at desired frequencies can be obtained. At first glance, it can be viewed as spiral structure where the outer structure resonates at lower frequencies and the inner structure will provide resonance at higher frequency. Thus, G-slot DSS provided a multi-band response, along with narrow bandstop response. The key observation for narrow multi-band response was to etch the slot till the edge of the power divider arm. The dimensions of power divider were maintained with length of G-slot changed to $l = 17.3$ mm with same width $w = 0.25$ mm and etched gap $g = 0.3$ mm as shown in figure 5.5

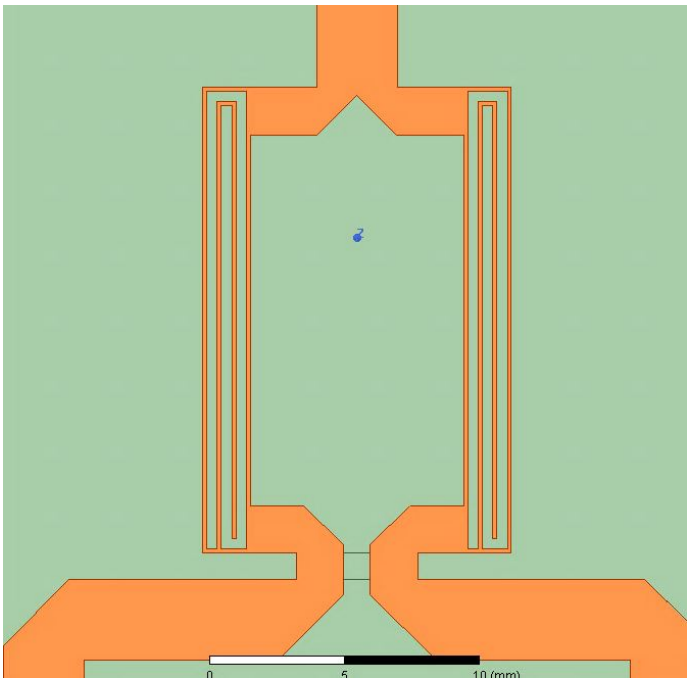

(a)

Figure 5.5: G slot etched till the edge design for narrow multi-band

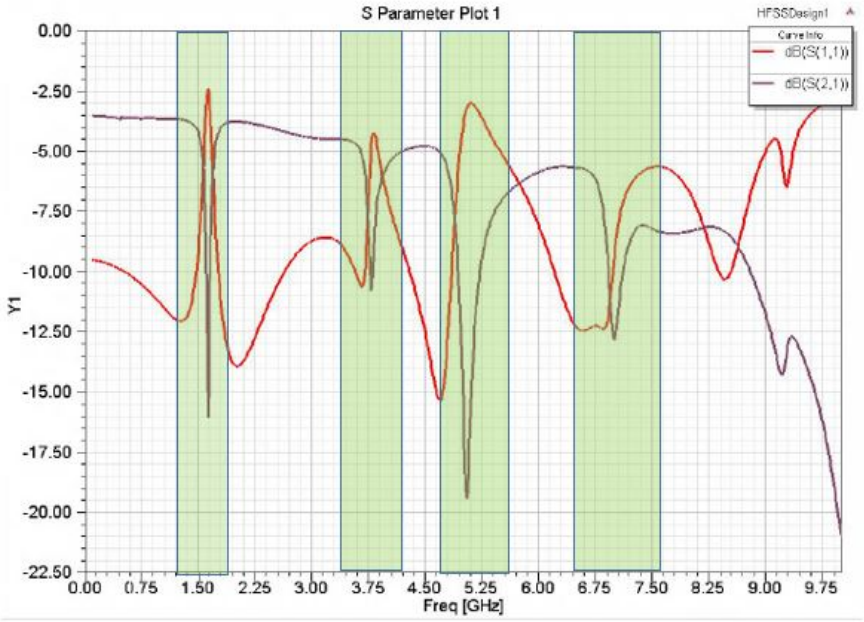

(a)

Figure 5.6: Simulated S-parameters for multiband response

The simulated results confirmed the presence of a multi band response. It was showed in the Figure 5.6 that the transmission loss S_{21} was -16dB at 1.6GHz , -11dB at 3.75 GHz ,-19.5 dB at 5.2 GHz and -12.5 dB at 7GHz. It also provided a very narrow bandstop, as it operated at 250 MHz to 1.5 GHz, then a bandstop at 1.6 GHz, and then again from 1.7 GHz to 2.75 GHz. Desired insertion loss, cutoff bandwidth and resonance frequencies can be achieved by choosing various combinations of slot length, width and etched gap. Again circuit was fabricated, measured and and he results were consistent with the simulated results as shown in Figure 5.7 and 5.8

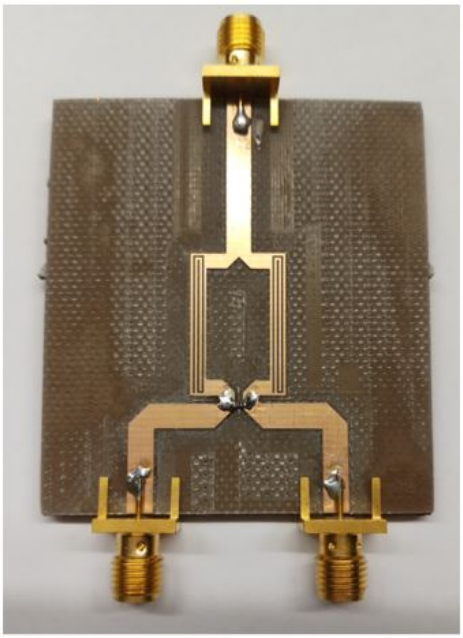

(a)

Figure 5.7: Fabricated G-slot etched till the edge design for narrow multi-band

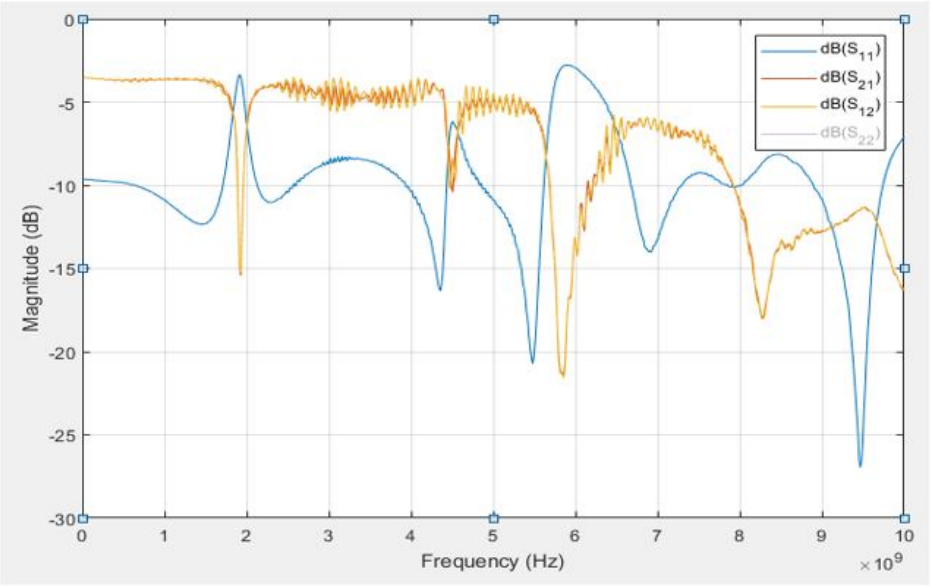

(a)

Figure 5.8: Measured S-parameters for multiband response

5.0.3 Frequency Selective Multi-band Response.

Another application was by integrating asymmetric DSS in different arms of the power divider. This led to different resonance frequencies at different outputs, which can have an application in feeding antennas or any other microwave circuits. Due to this technique, only one power divider was needed instead of two to get different resonating frequencies. The dimensions of the power divider are consistent here except for the G-slot length which was different for the left and right arm.The length of G-slot associated with port 2 was kept constant at a length $l = 17.3$ mm while the G-slot in other arm connected to port 3 was reduced to a length of $l = 8$ mm. The S-parameter simulated in Figure 5.10 was in agreement with the theory stated above as there were two different resonating frequencies at port 2 and port 3. Due to the longer slot length at port 2, the resonating frequency was at 1.7 GHz compared to port 3 which had smaller slot and resonated at 3.1 GHz. Both slots provided narrow bandstop response, as the return loss was -16dB at 1.7 GHz and -14 dB at 3.1 GHz, consistent with this theory. The Figure 5.9 showed the design in which only the length of one slot was reduced while keeping the other parameters the same. Figure 5.10 showed the S-parameter of this design depicting two resonance frequencies one at 1.75 GHz and the other at 3.25 GHz.

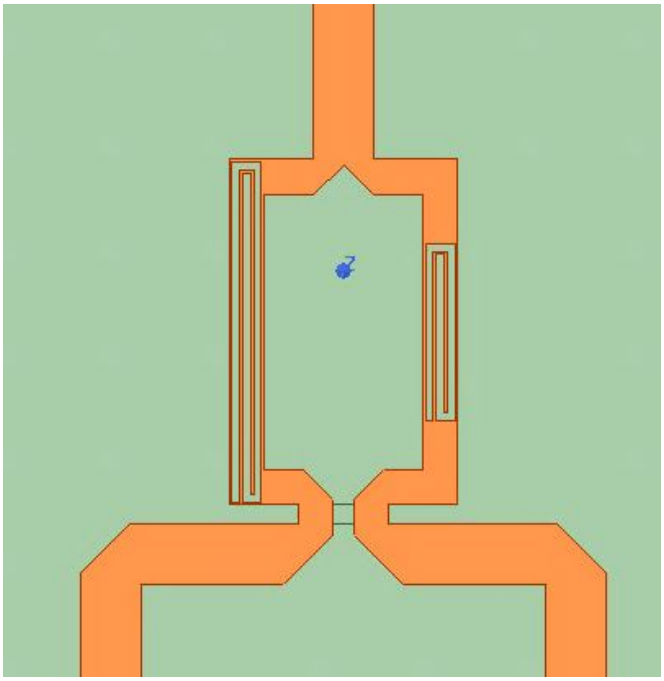

(a)

Figure 5.9: Asymmetric DSS slots

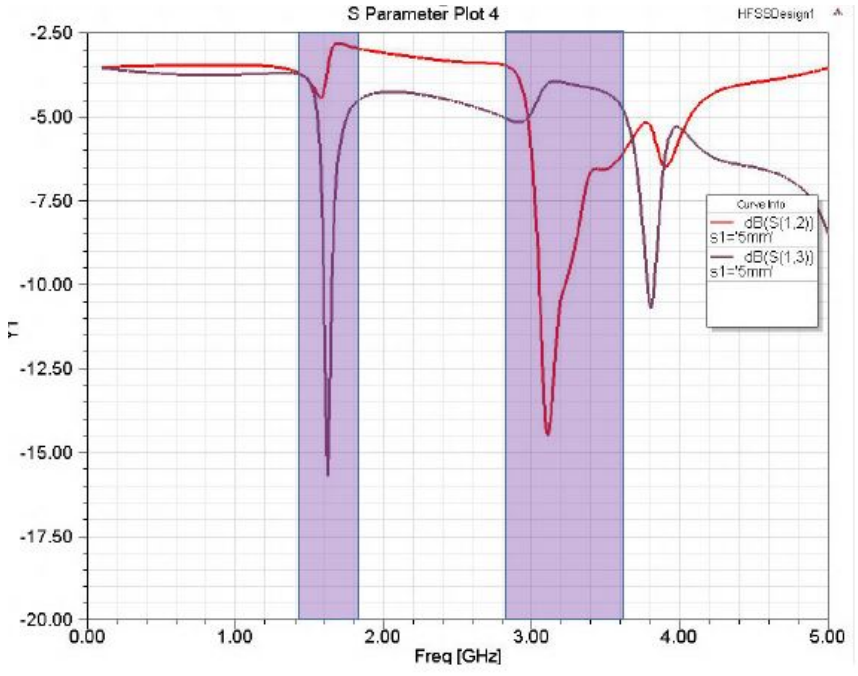

(a)

Figure 5.10: Asymmetric slot

Another degree of freedom sought with this design was to achieve different resonance frequencies at different output ports. The resonance frequency at a given output port can be customized by changing the dimensions of the slot in one arm, while keeping the slot in the other arm constant. Figure 5.11 showed that the length of the slot on one arm was kept constant while the length of the slot in the other arm got reduced. As expected, the insertion loss S_{21} was constant through the arm, where the slot length was kept constant and situated at the same frequency, independent of the slot length of other arm. While the resonating frequency was increasing in the arm, where the slot length was decreasing; hence the shifting in insertion loss S_{31}. This showed that the tuning of resonance can be achieved by using this design technique, and the resonance in ports were also independent from each other.

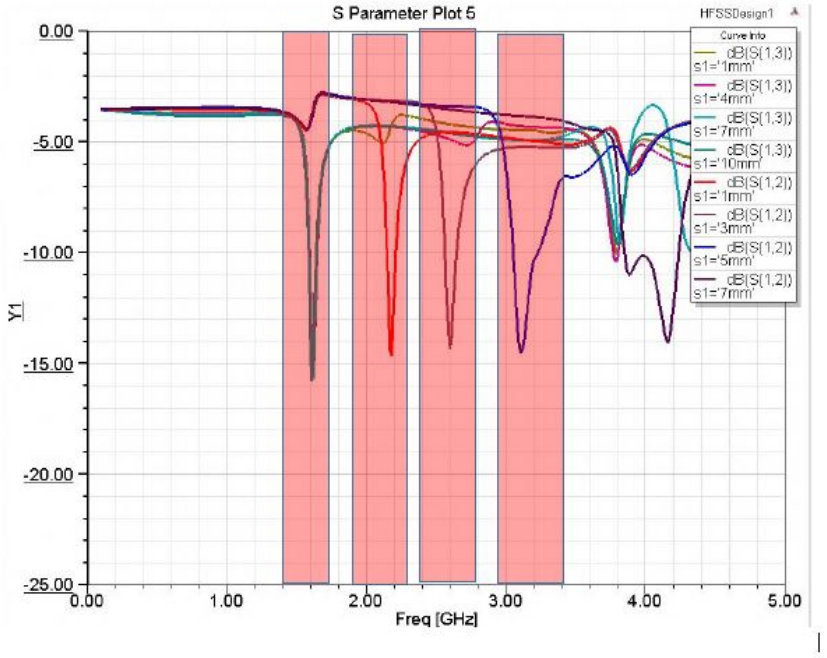

(a)

Figure 5.11: Frequency selective Multi-band response

5.0.3.1 Double U-slot DSS

The double U-slot DSS, shown in Figure 5.13, by inserting U slot in another U slot, introduces dual finite attenuation pole. Thus, a circuit was expected to resonate at two frequencies and achieve multi-band response [61]- [62]. The equivalent circuit of this multi-band resonator can be modeled as multi parallel RLC circuits shown in Figure 5.12

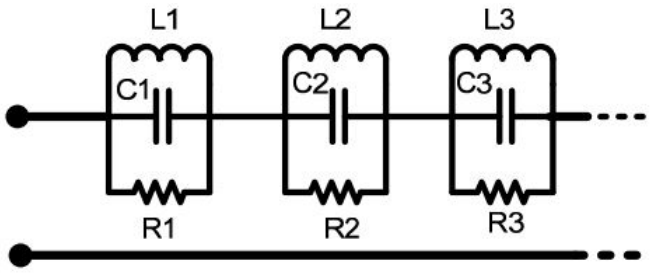

(a)

Figure 5.12: Circuit model of multi-band DSS [61]

The dimensions used for the power divider included a length of $l = 16.4$ mm and a width $w = 3.059$ mm for 50 Ω line and for the 70.7 Ω matching line the length was $l = 16.8$ mm and width $w = 1.8$ mm. The U-slots were of length $l = 12.75$ mm and space $c = g = w = 0.2$ mm. The simulated results were shown in Figure 5.14. It was evident from Figure 5.14 that attenuation of -23 dB and -33 dB at 3.5 Ghz and 7.0 GHz respectively can be achieved with these dimensions. Thus it provided a good multi-band response.

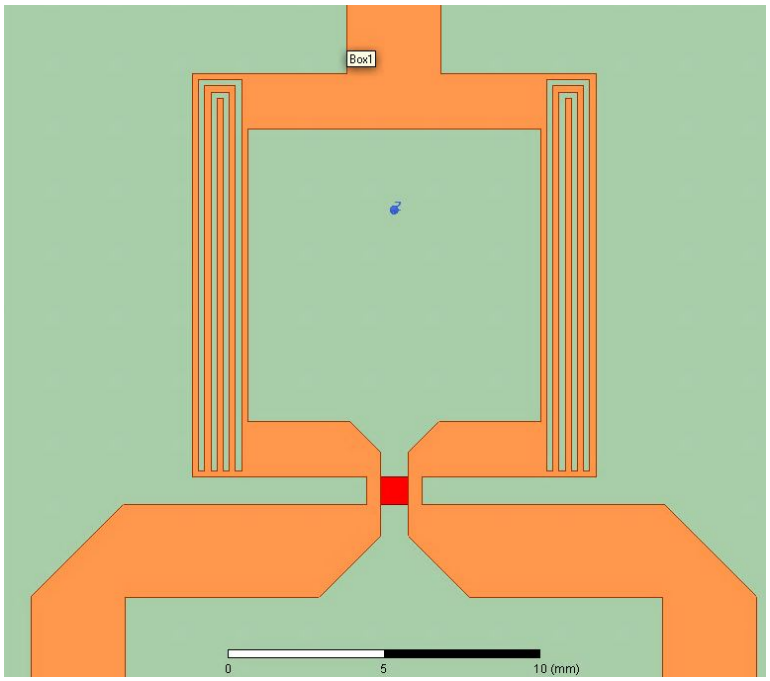

(a)

Figure 5.13: Design of double U-slot

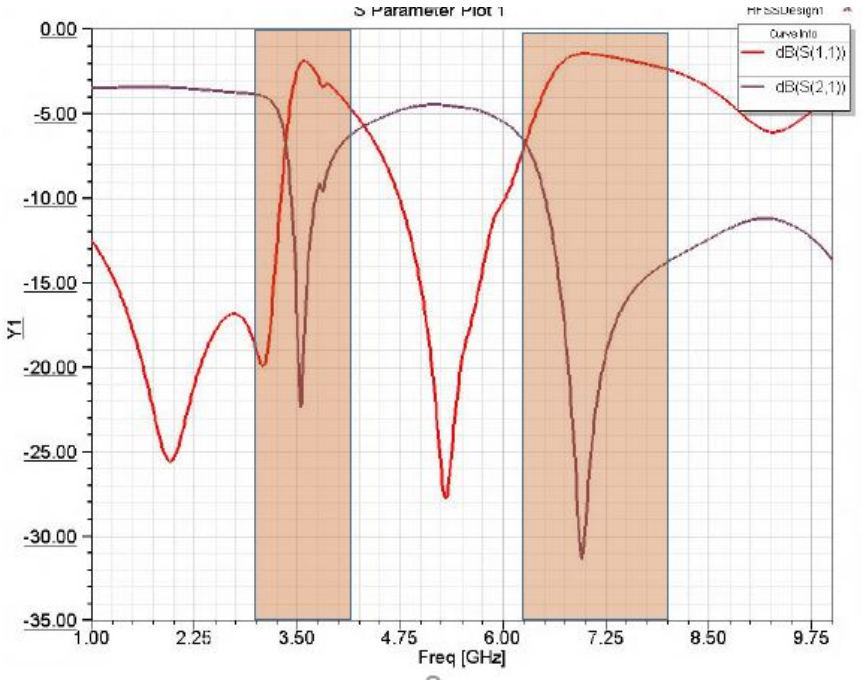

(a)

Figure 5.14: S-parameter for Double U-slot

Another notable property with this structure was that an additional notch could be created by reducing the length of inner U-slot as showed in Figure 5.15, and further illustrated by simulation showed in Figure 5.16. The length of outer and inner U-slot were 12.75 mm and 9.15 mm respectively. An additional notch at 5 GHz generated due to change in structure. It can also be observed that the other two nulls were not affected due to this change as compared to figure 5.14. Further tuning can be achieved by changing the length between two U slots. Thus, another degree of freedom can be attained by tuning the circuit by this technique. This was also showed in Figure 5.17, where only the length between the two slots was increased as a result nulls were created and shifted accordingly, by keeping main resonance fixed. This tuning technique required no additional space.

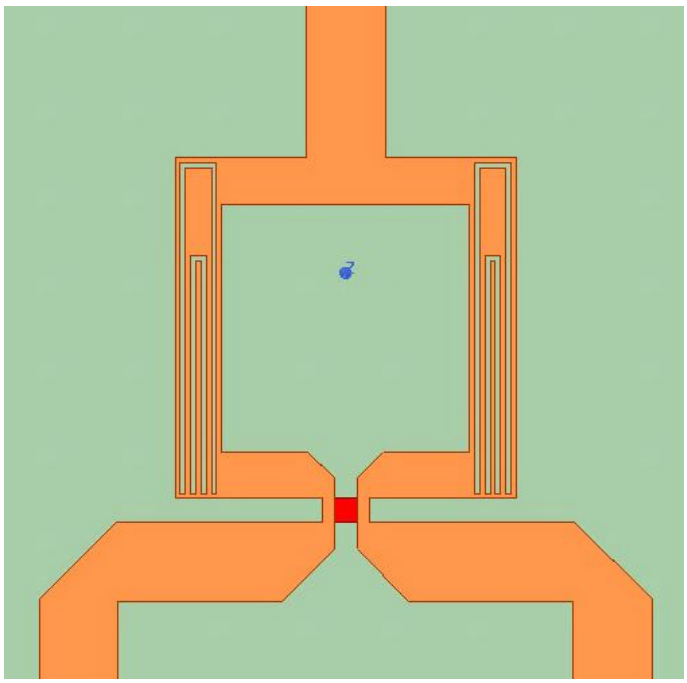

(a)

Figure 5.15: design of change in width between double U-slot

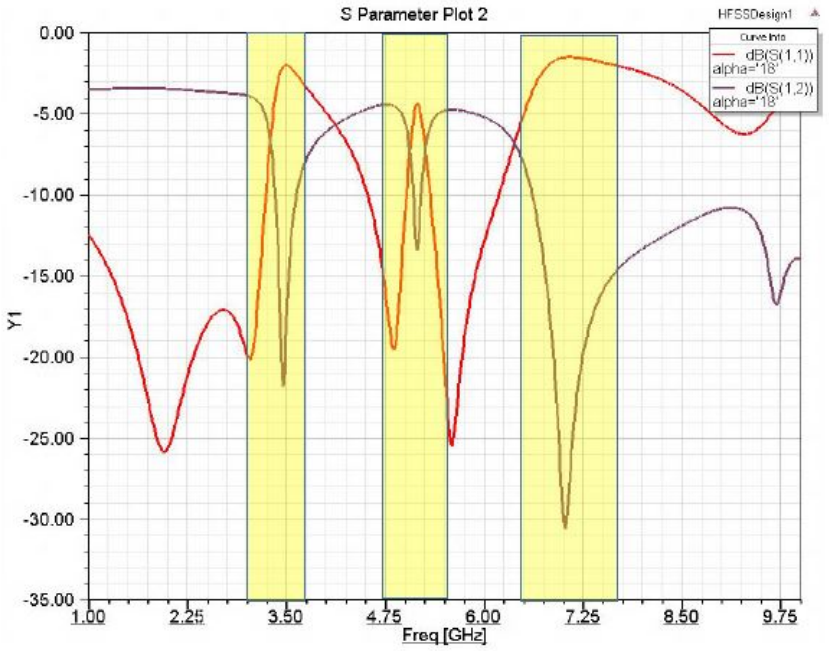

(a)

Figure 5.16: Change in width between double U-slot

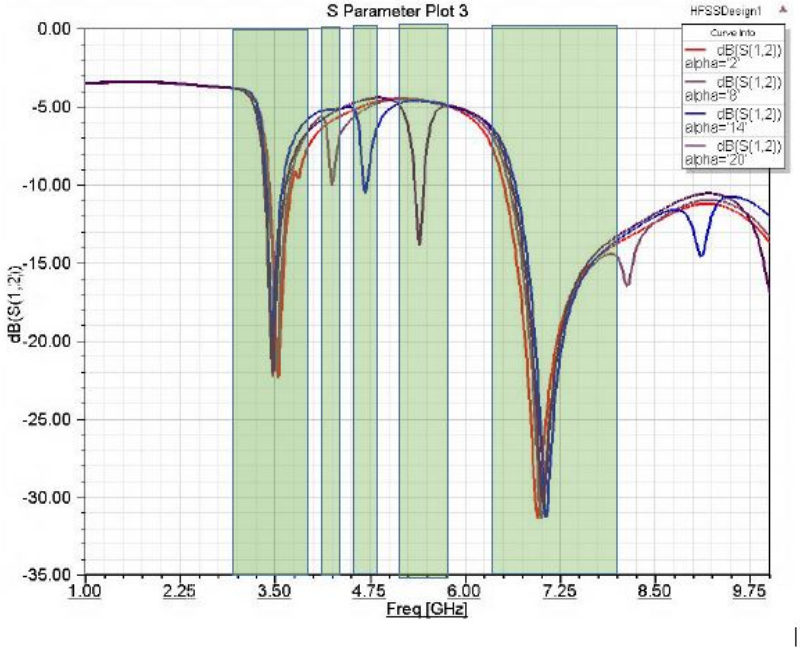

(a)

Figure 5.17: Increasing width between double U-slot

CHAPTER 6: CONCLUSIONS

In this thesis, a solution was provided, for achieving single-band and multi-band bandstop filtering response in a compact and cost effective way. To achieve this goal, the bandstop properties of electromagnetic bandgap (EBG) were exploited, where EM waves cannot propagate at certain frequency bands. Due to the complexity of modeling and parameter extraction in EBG, defected ground signal was analyzed. DGS have all the properties of EBG and also have simple equivalent circuit. DGS seems to be a good choice but it can be only applicable to standalone circuits. In group circuits, where ground plane is shared by many components, etching the ground plane for one component will impact the frequency response of other. Hence, defect in signal line was considered to solve this issue and make components independent from each other.

This document shows that the analysis, equivalent model and parameter extraction of Defected signal-line structure (DSS) was similar to defected ground structure (DGS). A U-slot was analyzed throughly, by also varying its length, width and gap and the results were consistent with the analysis of defected ground signal structures. Then a G-slot DSS was propose to achieve higher effective inductance and capacitance in a small area, it was also shown the dependence of DSS dimensions on effective inductance and capacitance. The last application section, where G-slot was integrated with single section Wilkinson power divider to achieve the objective of the thesis. First one was to get singleband bandstop frequency response at 2.4 GHz. It was shown that by changing the dimensions shifts the resonance frequency and hence the bandstop frequency response. The circuit was designed and fabricated and the results were in good agreement with the simulations. The second objective was to

attain narrow bandstop response along with multiband bandstop response. DSS slots were designed till the edges of power divider to get more effective inductance due to which desired response can be achieved. The third objective was to get tuning capability, so asymmetric slots in different arms of power divider were used to get resonance at multiple frequencies and they can be tunes by changing the dimensions of DSS.Thus, all the desired objectives were obtained.

For future work these structure can be integrated with antennas and other microwave circuits. They can be designed to achieve wide rejection in bandstop filtering. The other implementation could be on silicon substrates using MEMS switches to produce better performance and integration capability with RF integrated circuits.

REFERENCES

[1] AMICOM, "European $R\&D$ achievements in RF MEMS and RFMicrosystems", Workshop Europ. Microw. Week (EuMW), October 2007.

[2] R. Brown, C. D. Parker, and E. Yablonovitch, "Radiation properties of a planar antenna on a photonic-crystal substrate," J. Opt. Soc. Am. B 10, 404-407 (1993)

[3] Yongxi Qian, V. Radisic and T. Itoh, "Simulation and experiment of photonic band-gap structures for microstrip circuits," Proceedings of 1997 Asia-Pacific Microwave Conference, Hong Kong, 1997, pp. 585-588 vol.2.

[4] V. Radisic, Y. Qian, R. Coccioli and T. Itoh, "Novel 2-D photonic bandgap structure for microstrip lines," in IEEE Microwave and Guided Wave Letters, vol. 8, no. 2, pp. 69-71, Feb. 1998.

[5] V. Radisic, Y. Qian and T. Itoh, "Broad-band power amplifier using dielectric photonic bandgap structure," in IEEE Microwave and Guided Wave Letters, vol. 8, no. 1, pp. 13-14, Jan. 1998.

[6] V. Radisic, Yongxi Qian and T. Itoh, "Broadband power amplifier integrated with slot antenna and novel harmonic tuning structure," 1998 IEEE MTT-S International Microwave Symposium Digest (Cat. No.98CH36192), Baltimore, MD, USA, 1998, pp. 1895-1898 vol.3.

[7] Fei-Ran Yang, Yongxi Qian, R. Coccioli and T. Itoh, "A novel low-loss slow-wave microstrip structure," in IEEE Microwave and Guided Wave Letters, vol. 8, no. 11, pp. 372-374, Nov. 1998.

[8] K. -. Ma, K. Hirose, F. -. Yang, Y. Qian and T. Itoh, "Realisation of magnetic conducting surface using novel photonic bandgap structure," in Electronics Letters, vol. 34, no. 21, pp. 2041-2042, 15 Oct. 1998.

[9] Fei-Ran Yang, Kuang-Ping Ma, Yongxi Qian and T. Itoh, "A novel TEM waveguide using uniplanar compact photonic-bandgap (UC-PBG) structure," in IEEE Transactions on Microwave Theory and Techniques, vol. 47, no. 11, pp. 2092-2098, Nov. 1999.

[10] Chul-Soo Kim, Jun-Seok Park, Dal Ahn and Jae-Bong Lim, "A novel 1-D periodic defected ground structure for planar circuits," in IEEE Microwave and Guided Wave Letters, vol. 10, no. 4, pp. 131-133, April 2000.

[11] Jong-Sik Lim, Chul-Soo Kim, Jun-Seok Park, Dal Ahn and Sangwook Nam, "Design of 10 dB 90/spl deg/ branch line coupler using microstrip line with defected ground structure," in Electronics Letters, vol. 36, no. 21, pp. 1784-1785, 12 Oct. 2000.

[12] Insik Chang and Bomson Lee, "Design of defected ground structures for harmonic control of active microstrip antenna," IEEE Antennas and Propagation Society International Symposium (IEEE Cat. No.02CH37313), San Antonio, TX, USA, 2002, pp. 852-855 vol.2.

[13] Fei-Ran Yang, Kuang-Ping Ma, Yongxi Qian and T. Itoh, "A uniplanar compact photonic-bandgap (UC-PBG) structure and its applications for microwave circuit," in IEEE Transactions on Microwave Theory and Techniques, vol. 47, no. 8, pp. 1509-1514, Aug. 1999.

[14] Insik Chang and Bomson Lee, "Design of defected ground structures for harmonic control of active microstrip antenna," IEEE Antennas and Propagation Society International Symposium (IEEE Cat. No.02CH37313), San Antonio, TX, USA, 2002, pp. 852-855 vol.2.

[15] Jong-Im Park et al., "Modeling of a photonic bandgap and its application for the low-pass filter design," 1999 Asia Pacific Microwave Conference. APMC'99. Microwaves Enter the 21st Century. Conference Proceedings (Cat. No.99TH8473), Singapore, 1999, pp. 331-334 vol.2.

[16] Chul-Soo Kim, Jun-Seok Park, Dal Ahn and Jae-Bong Lim, "A novel 1-D periodic defected ground structure for planar circuits," in IEEE Microwave and Guided Wave Letters, vol. 10, no. 4, pp. 131-133, April 2000.

[17] T. Moyra, A. Roy, S. K. Parui and S. Das, "Design of 10 dB branch line coupler by using DGS," 2012 International Conference on Communications, Devices and Intelligent Systems (CODIS), Kolkata, 2012, pp. 516-519.

[18] Jong-Sik Lim, Ho-Sup Kim, Jun-Seek Park, Dal Ahn and Sangwook Nam, "A power amplifier with efficiency improved using defected ground structure," in IEEE Microwave and Wireless Components Letters, vol. 11, no. 4, pp. 170-172, April 2001.

[19] Jun-Seok Park, Jae-Ho Kim, Jong-Hun Lee, Sang-Hyuk Kim and Sung-Ho Myung, "A novel equivalent circuit and modeling method for defected ground structure and its application to optimization of a DGS lowpass filter," 2002 IEEE MTT-S International Microwave Symposium Digest (Cat. No.02CH37278), Seattle, WA, USA, 2002, pp. 417-420 vol.1.

[20] A. Boutejdar, A. Ramadan, M. Makkey and A. S. Omar, "Design of Compact Microstrip Lowpass Filters Using a U-Shaped Defected Ground Structure and Compensated Microstrip Line," 2006 European Microwave Conference, Manchester, 2006, pp. 267-270.

[21] Jong-Sik Lim, Chul-Soo Kim, Young-Taek Lee, Dal Ahn and Sangwook Nam, "A spiral-shaped defected ground structure for coplanar waveguide," in IEEE Microwave and Wireless Components Letters, vol. 12, no. 9, pp. 330-332, Sept. 2002.

[22] Duk-Jae Woo and Taek-Kyung Lee, "Suppression of harmonics in Wilkinson power divider using dual-band rejection by asymmetric DGS," in IEEE Transactions on Microwave Theory and Techniques, vol. 53, no. 6, pp. 2139-2144, June 2005.

[23] D. Woo, J. Lee and T. Lee, "Multi-band Rejection DGS with Improved Slow-wave Effect," 2008 38th European Microwave Conference, Amsterdam, 2008, pp. 1342-1345.

[24] Jong-Sik Lim, Young-Taek Lee, Chul-Soo Kim, Dal Ahn and Sangwook Nam, "A vertically periodic defected ground structure and its application in reducing the size of microwave circuits," in IEEE Microwave and Wireless Components Letters, vol. 12, no. 12, pp. 479-481, Dec. 2002.

[25] Abdel-Rahman, A. Boutejdar, A. K. Verma, G. Nadim and A. S. Omar, "Improved circuit model for DGS based lowpass filter," IEEE Antennas and Propagation Society Symposium, 2004., Monterey, CA, USA, 2004, pp. 998-1001 Vol.1.

[26] N. C. Karmakar, S. M. Roy and I. Balbin, "Quasi-static modeling of defected ground structure," in IEEE Transactions on Microwave Theory and Techniques, vol. 54, no. 5, pp. 2160-2168, May 2006.

[27] Jong-Sik Lim, Chul-Soo Kim, D. Ahn, Yong-Chae Jeong and Sangwook Nam, "Design of low-pass filters using defected ground structure," in IEEE Transactions on Microwave Theory and Techniques, vol. 53, no. 8, pp. 2539-2545, Aug. 2005.

[28] A. Boutejdar, A. Ramadan, M. Makkey and A. S. Omar, "Design of Compact Microstrip Lowpass Filters Using a U-Shaped Defected Ground Structure and Compensated Microstrip Line," 2006 European Microwave Conference, Manchester, 2006, pp. 267-270.

[29] A. Boutejdar, G. Nadim, S. Amari and A. S. Omar, "Control of bandstop response of cascaded microstrip low-pass-bandstop filters using arrowhead slots in backside metallic ground plane," 2005 IEEE Antennas and Propagation Society International Symposium, Washington, DC, 2005, pp. 574-577 vol. 1B.

[30] A. Boutejdar, A. Elsherbini and A. S. Omar, "A Compact Microstrip Multi-Layer Lowpass Filter Using Triangle Slots Etched in the Ground Plane," 2006 European Microwave Conference, Manchester, 2006, pp. 271-274.

[31] A. Boutejdar, A. Elsherbini and A. Omar, "A new cross-head defected ground structure (CDGS) for a compact low-pass filter with a wide stop-band," 2007 European Microwave Conference, Munich, 2007, pp. 842-845.

[32] A. Boutejdar, M. Makkey, A. Elsherbini, O. Luxor and A. Omar, "Design of compact extended-stopband microstrip low-pass filters by employing new mutual-coupling technique for defected ground structures (DGSs)," 2007 European Microwave Conference, Munich, 2007, pp. 71-74.

[33] J. D. Park, Y. J. Sung, S. H. Lee and Y. S. Kim, "Tunable bandstop filters using defected ground structure with active devices," 2005 Asia-Pacific Microwave Conference Proceedings, Suzhou, 2005, pp. 3 pp.-.

[34] R. Zhang and R. R. Mansour, "Novel tunable lowpass filters using folded slots etched in the ground plane," IEEE MTT-S International Microwave Symposium Digest, 2005., Long Beach, CA, 2005, pp. 4 pp.-778.

[35] R. Zhang and R. R. Mansour, "Novel digital and analogue tunable lowpass filters," in IET Microwaves, Antennas & Propagation, vol. 1, no. 3, pp. 549-555, June 2007.

[36] D. Pozar, Microwave Engineering, John Wiley & Sons Inc., Third edition, 2005

[37] E.J. Wilkinson, "An N-way Power Divider", IRE Trans. on Microwave Theory and Techniques, vol. 8, p. 116-118, Jan. 1960

[38] As recommended by the IEEE Standard Definitions of Terms for Radio Wave Propagation, IEEE Standard 211-1997, the terms "electric field" and "magnetic field" are used in place of the older terminology of "electric field intensity" and "magnetic field intensity"

[39] J. Reed and G. J. Wheeler, "A Method of Analysis of Symmetrical Four-Port Networks," in IRE Transactions on Microwave Theory and Techniques, vol. 4, no. 4, pp. 246-252, October 1956.

[40] E. O. Hammerstad, "Equations for Microstrip Circuit Design," Proceedings of the 5th European Microwave Conference, pp. 268-272, 1975.

[41] E. Yablonovitch, "Photonic band-gap structures," J. Opt. Soc. Am. B 10, 283-295 (1993)

[42] J. D. Joannopoulos, R. D. Meade, and J. N. Winn, "Electromagnetic modeling for microwave imaging of cylindrical buried inhomogeneities," Photonic Crystals, Princeton Univ. Press, Princeton, NJ, 1995

[43] D. F. Sievenpiper, M. E. Sickmiller, and E. Yablonovitch, "3D wire mesh photonic crystals," Phys. Rev. Lett., Vol. 76, No. 14, pp. 2480-2483, Apr. 1996.

[44] J. Shumpert, T. Ellis, G. Rebeiz, and L. Katehi, "Microwave and millimeter wave propagation in photonic band-gap structures," Proceeding of Ant. Prop. Symp. (AP-S), p. 678, 1997

[45] Y. Qian, V. Radisic, and T. Itoh, "Simulation and experiment of photonic band-gap structures for microstrip circuits," Proceeding of Asia-Pacific Microw. Conf. (APMC), pp. 585-588, 1997

[46] A. Yariv and P. Yeh, Optical Waves in Crystals, Wiley & Sons, 1984.

[47] E. Yablonovitch, "Inhibited spontaneous emission in solid state physics and electronics," Phys. Rev. Lett., Vol. 58, No. 20, pp. 2059-2062, 1987.

[48] Bao-qin Lin, Qiu-rong Zheng and Nai-chang Yuan, "A novel planar PBG structure for size reduction," in IEEE Microwave and Wireless Components Letters, vol. 16, no. 5, pp. 269-271, May 2006.

[49] E. R. Brown, C. D. Parker, and E. Yablonovitch, "Radiation properties of a planar antenna on a photonic-crystal substrate," J. Opt. Soc. Am. B 10, 404-407 (1993)

[50] M. M. Sigalas, R. Biswas, and K. M. Ho, "Theoretical study of dipole antennas on photonic band-gap materials," Microwave Opt. Technol. Lett., Vol. 13, No. 4, pp. 205-209, Nov. 1996.

[51] H. -. D. Yang, N. G. Alexopoulos and E. Yablonovitch, "Photonic band-gap materials for high-gain printed circuit antennas," in IEEE Transactions on Antennas and Propagation, vol. 45, no. 1, pp. 185-187, Jan. 1997.

[52] R. D. Meade, K. D. Brommer, A. M. Rappe, and J. D. Joannopoulos, "Photonic bound states in periodic dielectric materials," Phys. Rev. B., Vol. 44, No. 24, pp. 13772-13774, Dec. 1991.

[53] L. H. Weng, Y.-C. Guo, X.-W. Shi, and X.-Q. Chen, "An Overview on Defected Ground Structure," Progress In Electromagnetics Research B, Vol. 7, 173-189, 2008.

[54] Jong-Im Park et al., "Modeling of a photonic bandgap and its application for the low-pass filter design," 1999 Asia Pacific Microwave Conference. APMC'99. Microwaves Enter the 21st Century. Conference Proceedings (Cat. No.99TH8473), Singapore, 1999, pp. 331-334 vol.2.

[55] Jong-Sik Lim, Chul-Soo Kim, D. Ahn, Yong-Chae Jeong and Sangwook Nam, "Design of low-pass filters using defected ground structure," in IEEE Transactions on Microwave Theory and Techniques, vol. 53, no. 8, pp. 2539-2545, Aug. 2005.

[56] G. L. Matthaei, L. Young, and E. M. T. Jones, Microwave Filters,Impedance-Matching Networks, and Coupling Structures. Dedham,MA: Artech House, 1980

[57] Insik Chang and Bomson Lee, "Design of defected ground structures for harmonic control of active microstrip antenna," IEEE Antennas and Propagation Society International Symposium (IEEE Cat. No.02CH37313), San Antonio, TX, USA, 2002, pp. 852-855 vol.2.

[58] Jun-Seok Park, Jae-Ho Kim, Jong-Hun Lee, Sang-Hyuk Kim and Sung-Ho Myung, "A novel equivalent circuit and modeling method for defected ground structure and its application to optimization of a DGS lowpass filter," 2002 IEEE

MTT-S International Microwave Symposium Digest (Cat. No.02CH37278), Seattle, WA, USA, 2002, pp. 417-420 vol.1.

[59] Jun-Seok Park, Jae-Ho Kim, Jong-Hun Lee, Sang-Hyuk Kim and Sung-Ho Myung, "A novel equivalent circuit and modeling method for defected ground structure and its application to optimization of a DGS lowpass filter," 2002 IEEE MTT-S International Microwave Symposium Digest (Cat. No.02CH37278), Seattle, WA, USA, 2002, pp. 417-420 vol.1.

[60] Duk-Jae Woo, Taek-Kyung Lee, Jae-Wook Lee, Cheol-Sig Pyo and Won-Kyu Choi, "Novel U-slot and V-slot DGSs for bandstop filter with improved Q factor," in IEEE Transactions on Microwave Theory and Techniques, vol. 54, no. 6, pp. 2840-2847, June 2006.

[61] S. Fallahzadeh, A. Molaei and A. Cheldavi, "Microstrip Wilkinson power divider with multi-spurious suppression," IEEE Middle East Conference on Antennas and Propagation (MECAP 2010), Cairo, 2010, pp. 1-3.

[62] Sio-Weng Ting, Kam-Weng Tam and R. P. Martins, "Miniaturized microstrip lowpass filter with wide stopband using double equilateral U-shaped defected ground structure," in IEEE Microwave and Wireless Components Letters, vol. 16, no. 5, pp. 240-242, May 2006.